Quantifying Head Motion Associated with fMRI Motor Tasks

by

Emily Seto

A thesis submitted in conformity with the requirements
For the degree of Master of Science
Graduate Department of Medical Biophysics
University of Toronto

Quantifying Head Motion Associated with fMRI Motor Tasks

Degree of Master of Science 2000
Emily Seto
Department of Medical Biophysics
University of Toronto

Abstract

Head motion is a frequent problem in functional magnetic resonance imaging (fMRI) studies due to long experiment times, small signal changes associated with brain activation, and head motion produced by behavioural tasks. Current methods to minimize and correct for head movement do not completely solve the problem, particularly for specific patient populations. Head motion characteristics of stroke subjects, age-matched controls and young adults were investigated using an MR simulator and a highly accurate position tracking system. It was found that head motion strongly depended upon the subject group and less upon the task conditions. The stroke subjects exhibited approximately twice the head motion compared to that of the age-matched controls. The latter's head motion was about twice that of the young adults. The dominant translational and rotational directions of head motion were superior-inferior and pitch (nodding), respectively. This work has important implications for improving the quality of fMRI.

Acknowledgements

I would like to express my gratitude to the numerous people without whose assistance and advice, this work would not have been possible. Dr. Bill McIlroy, Dr. Sandra Black, Dr. Richard Staines, and all the others in the fMRI group have provided me with invaluable technical support and guidance. I would like to thank Cathy Nangini for her continuous help with the equipment and data acquisition, and Gal Sela for sharing his technical expertise. I also thank my supervisory committee members, Dr. Peter Burns, Dr. Mike Bronskill, and especially Dr. Randy McIntosh for his time and advice on data analyses. I would like to give a special thanks to my supervisor, Dr. Simon Graham, for his tireless help, patience, and guidance throughout all aspects of this thesis. Finally, a full hearted thanks to my family and my dear friends for their greatly appreciated moral support and encouragement.

Table of Contents

List of Tables and Figures

Figures

Tables

Chapter 1

Introduction

For the past decade, functional magnetic resonance imaging (fMRI) has been used to study how the brain operates [1, 2, 3, 4]. This imaging technique has proven highly successful, and is now a major experimental tool in neuroscience. Despite this success, fMRI remains an immature method and there is strong potential for improving the methodology. In particular, fMRI is well known to be sensitive to image artifacts arising from head motion. Although numerous artifact correction methods have been proposed, they do not completely solve the problem. Surprisingly, little quantitative information is known about the nature of head motion during fMRI scans. This thesis provides a detailed investigation of head motion during behavioural tasks for a spectrum of volunteers that is typical in fMRI research applications: young healthy adults, healthy seniors, and patients with neurodisability. The goal of this work is to provide the information required to improve designs of head stabilization and future motion correction techniques.

This first chapter reviews background information that provides the rationale for the project, and ends with the specific goals that will be addressed. Chapter 2 presents the experimental method, results, and impact of the research. Chapter 3 summarizes the conclusions that can be drawn and examines future directions worth investigating.

1.1 functional MRI

1.1.1 Role of fMRI in Functional Neuroimaging

In the past few decades, minimally invasive methods of investigating brain function have been developed. The main techniques include electroencephalography (EEG), magnetoencephalography (MEG), positron emission tomography (PET), and fMRI. Electroencephalography and MEG have very high temporal resolution (sub-millisecond), but poor spatial resolution (centimeters) as well as limited brain depth penetration. In contrast, PET and fMRI have much higher spatial resolution (millimeters), can provide functional images of the entire brain volume, but are limited in temporal resolution. For PET, temporal resolution is limited by the uptake and radioactive decay of tracers injected into the blood stream, whereas for fMRI, temporal resolution is limited to approximately seconds by the latency of the hemodynamic response (changes in blood parameters, such as regional blood flow, from increased neuronal function) [5], although newer techniques are improving on this capability [6]. Functional MRI also offers a number of practical advantages. Unlike PET, fMRI is completely non-invasive. Although PET is generally more sensitive than fMRI, fMRI is cheaper and more readily available because it can be performed with the large installed base of existing magnetic resonance (MR) scanners that are used for radiological imaging in hospitals. Functional MRI also has a slightly higher spatial resolution than PET.

Although fMRI is an important tool in basic neuroscience research, it is also beginning to have a clinical impact. One of the first applications is in defining functional neuroanatomy for presurgical planning. Identifying brain regions with great functional importance could alter the surgical approach, such as that used for removal of a brain tumor [7]. It has been shown, for example, that locating the central sulcus (the site of primary

sensorimotor cortex) from anatomical MR images can be a difficult task in normal subjects and especially for patients with intracranial lesions [8]. By instructing the patient to perform a motor task, such as opening and closing his/her hand [9] during fMRI, functional localization can be performed effectively.

1.1.2 Fundamental MRI Physics

A brief summary of the pertinent signal contrast mechanisms and MR imaging principles is now presented as a knowledge base for the subsequent explanation of the physical aspects behind fMRI [1, 10].

1.1.2.1 Signal Contrast

The signal contrast in MRI is primarily achieved through the differences in concentration of hydrogen nuclei found in water molecules in tissues, as well as the molecular dynamics of water molecules. Hydrogen nuclei (protons) possess a small magnetic moment, such that if a strong static magnetic field is present, more protons will align parallel to the magnetic field compared to other orientations, resulting in a net equilibrium magnetization in this "longitudinal" direction. The magnetic moment of protons arises in part because of nuclear spin angular momentum. The protons do not align statically with an external magnetic field but precess, similar to a top spinning at an angle to the earth's gravitational field (Fig.1.1a). The "Larmor frequency" of precession, is proportional to the magnetic field and equals 42.58 MHz/Tesla for protons. Under these conditions, the protons do not precess in synchrony. The longitudinal magnetization is thus small, whereas the vectorial component of "transverse" magnetization in the plane orthogonal to the external

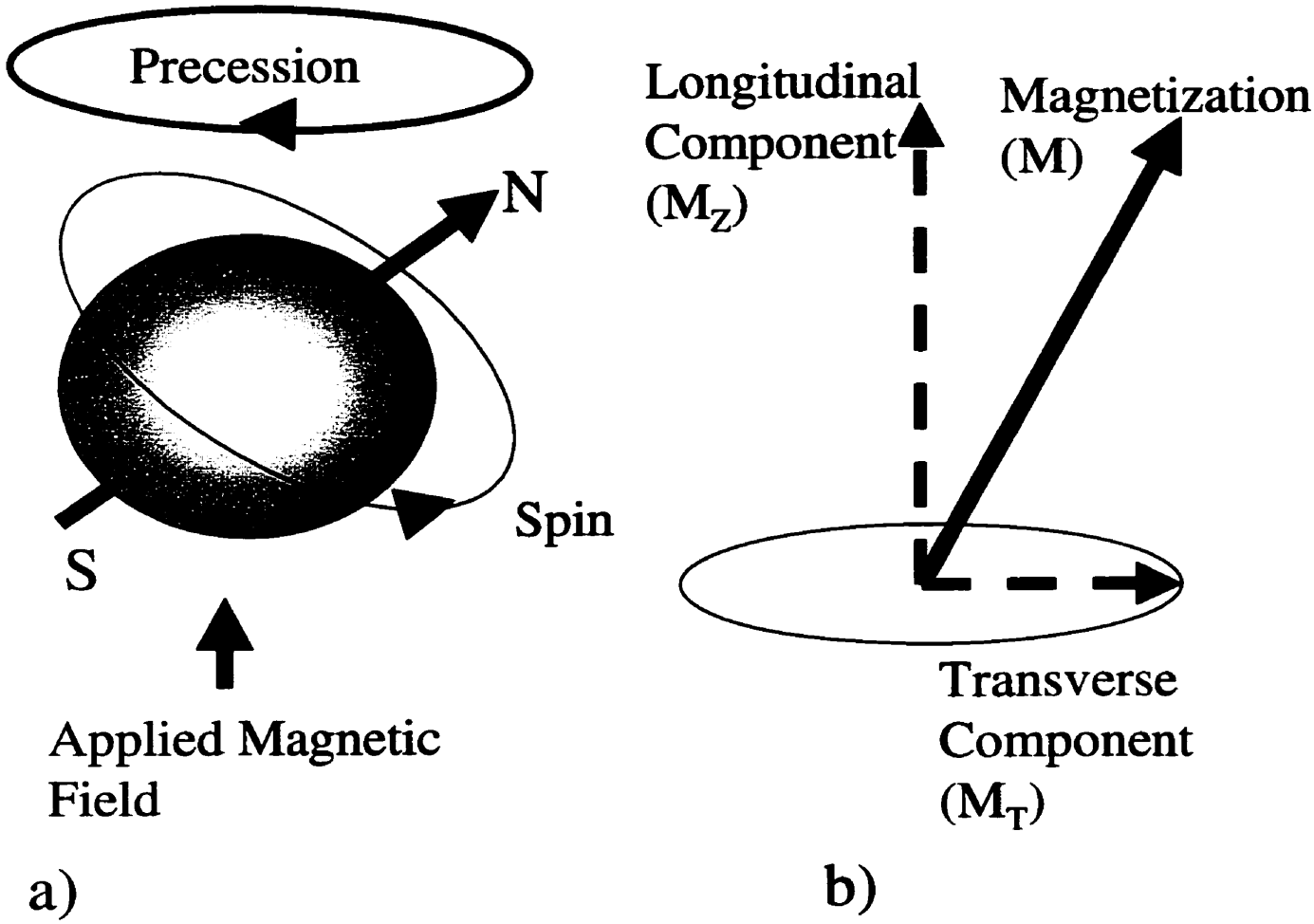

Figure 1.1. Proton has angular momentum ('spin') and small magnetic dipole moment (orientation shown by arrow and North-South symbols). An applied magnetic field causes precession (a). The net magnetization produced by a collection of protons (shown here with arbitrary orientation) can be decomposed into longitudinal and transverse components (b).

magnetic field (Fig. 1.1b) is zero.

If a radiofrequency (RF) "excitation" pulse orthogonal to the main magnetic field is applied at the Larmor frequency, it causes the protons to absorb energy and to precess coherently together (also referred to as being "in-phase"). The excited magnetization thus precesses at an increasing nutation angle, tipping from the longitudinal direction toward the transverse plane. As a result of this process, the magnetization achieves a transverse vectorial component that can be measured, when the RF pulse is turned off, as a voltage induced in an appropriately oriented receiver coil. The angle that the magnetization tips is known as the flip angle and is dependent on the RF pulse characteristics (amplitude, shape, and duration) (Fig. 1.2).

When the RF pulse is turned off, the magnetization eventually returns to the longitudinal equilibrium condition. The return is characterized by two fundamental MR parameters that govern the MR signal: the longitudinal relaxation rate (1/T1) and the transverse relaxation rate (1/T2). T1 (approximately 100 milliseconds to seconds for tissues) characterizes the return to equilibrium along the longitudinal direction. The recovery of longitudinal magnetization has a time dependence described by:

$$M_z(t)=M_0+(M_z(0)-M_0)e^{-t/T1} \qquad [1.1]$$

where M_0 is the equilibrium magnetization, $M_z(0)$ is the longitudinal magnetization immediately after the RF pulse is finished, and t is time.

T2 describes the decay rate of transverse magnetization, and the associated T2 values are typically less than those of T1 (approximately tens to hundreds of milliseconds for tissues). Transverse decay is caused by many factors (*eg* diffusion), although the main effect arises because protons on neighbouring water molecules cause inhomogeneities in the local

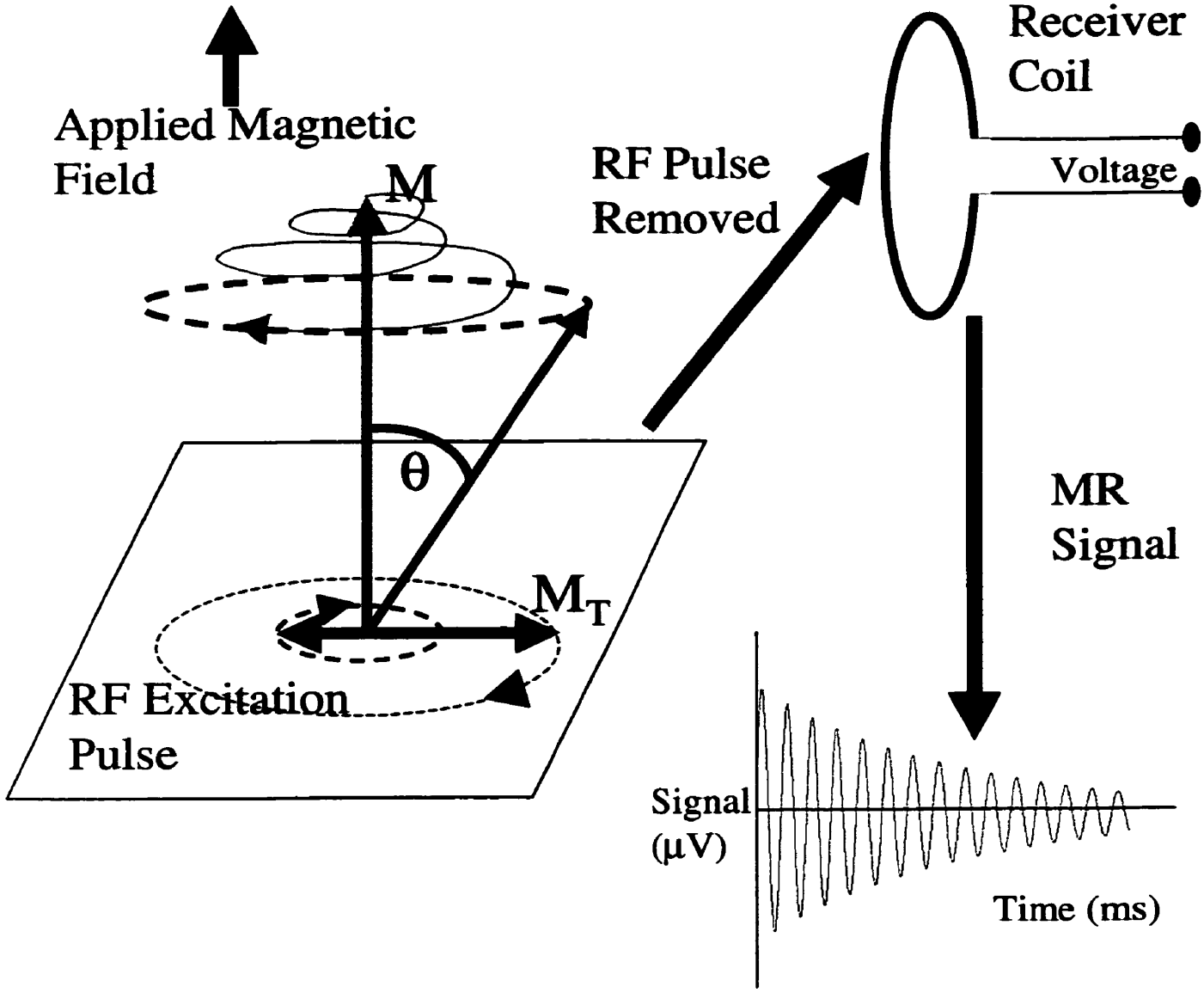

Figure 1.2. RF pulse (a small rotating magnetic field) causes protons to precess in-phase. Magnetization nutates to a "flip angle" (θ) and thus a rotating transverse component develops. When the RF pulse is removed, a receiver coil is used to measure the decaying MR signal as the transverse magnetization decreases.

magnetic field. Protons therefore precess at slightly different rates, resulting in loss of phase coherence (dephasing) that depends on molecular dynamics. Macroscopically, this leads to a transverse magnetization decay described by:

$$M_{xy}=M_{xy}(0)e^{-t/T2} \qquad [1.2]$$

where $M_{xy}(0)$ is the transverse magnetization right after removal of the RF pulse (t=0).

Another factor that enhances decay of the transverse magnetization arises from spatial inhomogeneity of the main magnetic field. The amount of field inhomogeneity depends on differences in bulk magnetic susceptibility (ratio of magnetization in a substance to the corresponding magnetizing force) within the tissue and the geometry. The most severe inhomogeneity occurs near the boundaries between two materials with differing susceptibilities, such as air and tissue (*ie* water is slightly diamagnetic, and air is slightly paramagnetic). When techniques to eliminate the effects of large-scale magnetic field inhomogeneities are not used, the observed transverse signal decay rate is denoted as 1/T2* (T2* ranges from a few to tens of milliseconds in tissues), to distinguish it from the intrinsic T2 value of the tissues being imaged. The MR signal S(t) decays according to the following formula:

$$S(t)=S_0e^{-t/T2^*} \qquad [1.3]$$

where S_0 is the initial signal strength following the RF pulse. Tissues with different T2*s can, therefore, be distinguished from each other because those with a long T2* will have a larger signal than those with a shorter T2* prior to complete decay of the signal [10].

1.1.2.2 Basic Imaging

The discussion so far has described MR signal characteristics that apply to homogenous tissue samples. To form an MR image that depicts the spatial structure of tissue anatomy, three mutually orthogonal sets of electromagnetic "gradient coils" are used for encoding magnetization spatially. First, a plane of the tissue to be imaged is selected. In order to excite only a thin slice of the tissue, a gradient is applied during the RF excitation. As previously mentioned, the frequency of the RF pulse must be at the Larmor frequency for excitation to occur. The temporal frequency bandwidth of the RF pulse can therefore be chosen to match the bandwidth of Larmor frequencies of the protons in the slice of interest.

Now that only a slice of the tissue is excited, 2-dimensional spatial encoding is necessary to form an image. As discussed above, the proton precession frequency is linearly dependent on the magnetic field. If the MR signal from tissues is acquired in the presence of a magnetic field with linearly increasing magnitude along a particular direction (a gradient), then the spatial components of the MR signal in this direction can be determined by frequency analysis (typically a Fourier Transform). To increase the coherence and strength of the MR signal, MR echoes can be generated that remove space-variant phase shifts momentarily (to get the precession back in-phase). There are in general two types of echoes: gradient and spin echo. Gradient echoes remove phase shifts from gradient fields, and spin echoes remove phase shifts from field inhomogeneities. [10] When spatial encoding is performed using two orthogonal gradients, the MR signal maps spatial frequency information on a 2-dimensional plane, called "k-space", with ordinate and abscissa coordinates represented in units of inverse position (*eg* cm^{-1}). The MR signal in k-space consists of complex numbers, the magnitude and phase of which characterize complex sinusoids of

specific spatial frequency and amplitude. The final image is produced from the 2-dimensional inverse Fourier Transform of the MR signal in k-space.

A single MR image usually requires many repeated RF excitation pulses and MR signal acquisitions because it is difficult to switch the gradient coils on and off quickly enough to trace a complete path through k-space before the MR signal has died out. This leads to imaging times of approximately minutes, because time is required for the magnetization to recover sufficiently in the longitudinal direction prior to the subsequent excitation. For example, in conventional "spin-warp imaging" used for most clinical anatomical MRI, each RF excitation results in acquisition of a single line in k-space.

It is usually desirable to take multiple slices of the brain. Even full brain coverage is achievable with some trade-offs. In particular, repetition time (TR, which is the time between successive excitations and in this case, for data acquisition of a single time point of a complete tissue volume) is usually increased because additional time is needed to acquire data from each slice. When an "image" is mentioned below, it encompasses the possibility of multiple slices of the brain.

1.1.3 Signal Contrast Mechanisms for fMRI

Several MR-based signal contrast mechanisms (*eg* blood perfusion [11], apparent diffusion of water molecules [12], and neuronal metabolism [13]) can be used to image brain activation (*ie* areas of increased neural function resulting from sensory stimuli or behavioural tasks, compared to resting state). Functional MRI usually exploits the BOLD (blood oxygenation level dependent) effect [14] because it is the most sensitive [15]. When an area of the brain activates, there is a local increase in the regional cerebral blood flow (rCBF),

cerebral blood volume (rCBV), and oxygen consumption (OC). These effects are known as a hemodynamic response. The increase in the OC (≈5%) rate is much smaller than the increase in the rCBF (≈50%) [2]. This results in an absolute decrease in the deoxyhemoglobin, which is paramagnetic (meaning that deoxyhemoglobin alters the magnetic field in its vicinity). On the other hand, oxyhemoglobin is diamagnetic and does not distort the magnetic field. Magnetization, associated with water molecules exchanging through increasingly oxygenated blood cells, plasma, and in nearby tissue, is irreversibly dephased by microscopic magnetic field inhomogeneity. The decrease in deoxyhemoglobin results in an increase in T2 and T2*. A small signal increase in the region of the neuronal activation therefore develops. The fractional signal change in cortical gray matter (2-4% over field strengths from 1.5 to 4 T) has been found to increase as the 1.6 power of the static field [16]. T2* is used for BOLD fMRI instead of T2 because it exhibits larger changes with blood oxygenation status. Gradient echo imaging is therefore almost always used when performing fMRI.

1.1.4 How fMRI is Performed

A time series of "snap-shot" fMR images (each approximately 50 ms) is taken to sample the hemodynamic response dynamically during time intervals when brain activation is increased, as well as during the rest intervals of behavioural tasks. It is now possible, using fast switching gradient coils (*eg* 4 mT/m/s), to create a "snap-shot" MR image in tens of milliseconds by traversing k-space completely with a single RF pulse, at the cost of some spatial resolution [9]. The two most commonly used image data acquisition techniques for fMRI are echo-planar imaging (EPI) and spiral imaging [17]. A TR on the order of a second is necessary to allow for the longitudinal relaxation of the magnetization and multislice

acquisition. Echo-planar imaging involves a Cartesian scan of k-space with a raster-like traversal. Spiral imaging involves radial traversal of k-space from the origin spiraling outward. One common spiral traversal involves the Archimedean spiral, given by:

$$k(t) = A\tau(t)e^{i\omega\tau(t)} \qquad [1.4]$$

where $\tau(t)$ is some function of time, $i=\sqrt{-1}$, ω is the angular frequency of the spiral, and A is a constant. Ideally, $\tau(t)=\sqrt{t}$ for a constant linear velocity spiral. A constant linear velocity spiral allows the acquired k-space data to be spread out relatively evenly, and the scan can be completed as quickly as possible [18]. Spiral trajectories are typically regridded to Cartesian coordinates to allow efficient Fourier Transformation. The k-space trajectories are shown in Fig. 1.3a and b for both types of imaging.

There is no clear consensus whether EPI or spiral imaging is better for fMRI, because each has its own advantages. Spiral imaging is superior in terms of motion insensitivity and, thus, provides a better "snap-shot" image because the low spatial frequencies are all acquired at the beginning of the acquisition [19, 20]. EPI, however, is slightly faster than spiral imaging. Both methods of traversing k-space are limited by the time necessary for the gradient coils to change the magnetic field gradient, but the raster-like pattern of EPI is less taxing on the switching of the gradient coils compared to spiraling outward in k-space. Echo planar imaging is, therefore, less sensitive to spatial inhomogeneity of the main magnetic field (*eg* magnetic susceptibility arising from air-bone interfaces) because a shorter acquisition time leads to less error accrual. Figure 1.3c and d compare "snap-shot" images acquired for fMRI with EPI and spiral imaging, respectively. Increased signal loss and

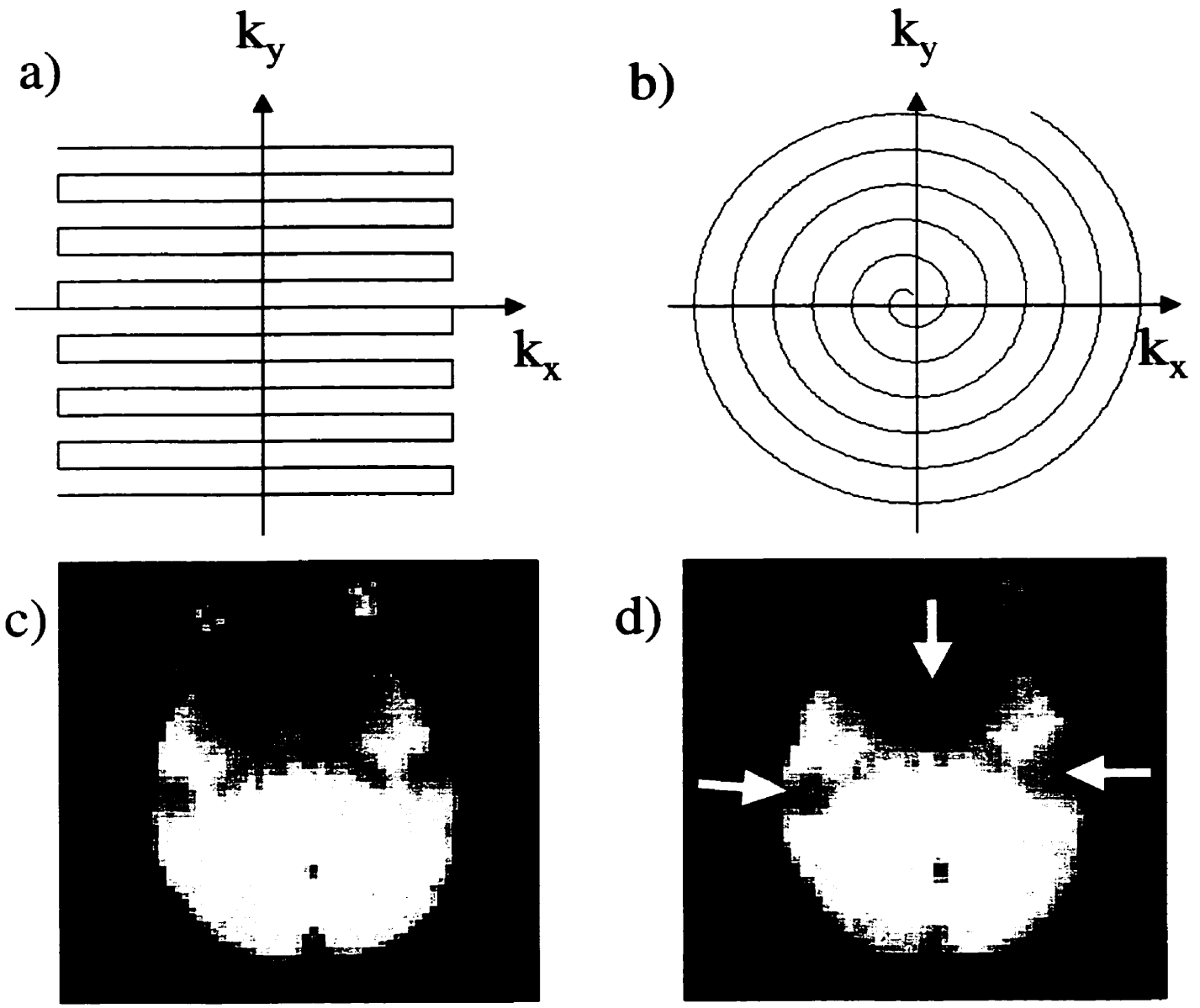

Figure 1.3. EPI (a) and spiral (b) data acquisition trajectory in k-space, and snap-shot axial images using EPI (c) and spiral (d) of the same brain anatomy. Note the increased artifacts from susceptibility effects around the nasal cavity and ear canal of the spiral image (arrows). [TR=2 s, echo time TE=40 ms, flip angle=80°, 5 mm slice, 64x64 matrix, field of view FOV=20 cm]

distortion near the nasal cavity is observed with spiral imaging.

To create a typical image of brain activation with fMRI, several hundred fast MR images are acquired within 5-10 minutes during multiply repeated behavioural tasks. The repetitions are necessary because the BOLD signal is intrinsically small and necessitates signal averaging, particularly at 1.5 T. Behavioural tasks are typically arranged in "blocked format", with continuously repeated executions of a task for a fixed duration of 15-30 s alternated with rest intervals of similar duration, or as "event-related" experiments, with brief stimulus/task events (approximately 1 s duration) alternating with rest intervals typically of 10 s duration. The following discussion is restricted to blocked format because it is more sensitive to finding regions of activation for clinical studies. Event-related fMRI does have some methodological advantages, however, such as exploiting the time lag of the hemodynamic response to wait for task-induced head motion to subside before acquisition of the fMRI data [21, 22].

For blocked design fMRI, functional images are constructed most commonly by first computing the correlation coefficient (cc) of the time series of each voxel compared to the idealized task pattern waveform (Fig.1.4). A voxel is deemed to be activated if the cc is above a statistical threshold chosen at an adequate confidence of significance (*eg* cc=0.3). The correlation coefficient can be written as:

$$cc = \frac{\sum_{i=1}^{N}(f_i - \mu_f)(r_i - \mu_r)}{\left[\sum_{i=1}^{N}(f_i - \mu_f)^2\right]^{1/2}\left[\sum_{i=1}^{N}(r_i - \mu_r)^2\right]^{1/2}} \qquad [1.5]$$

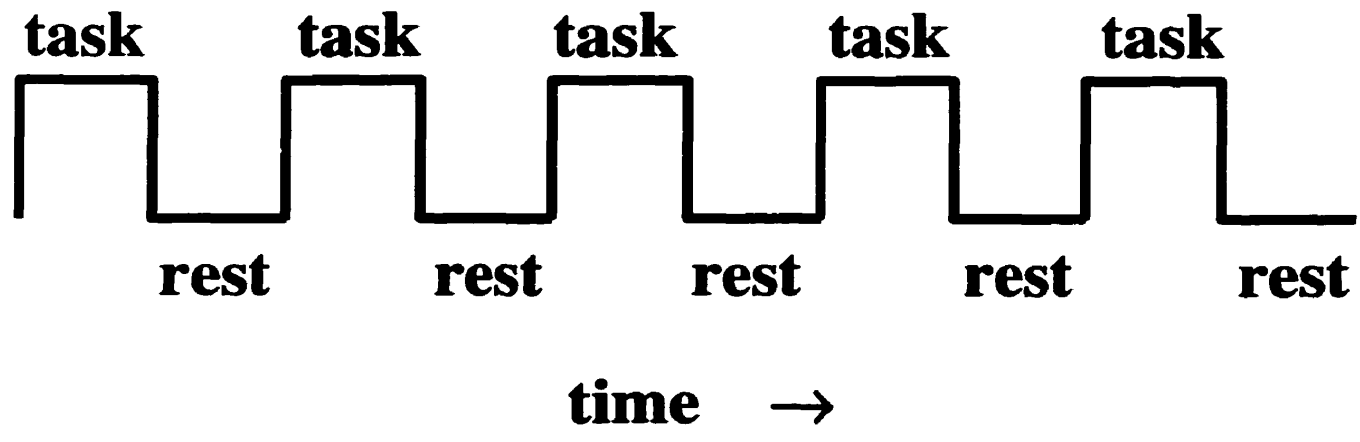

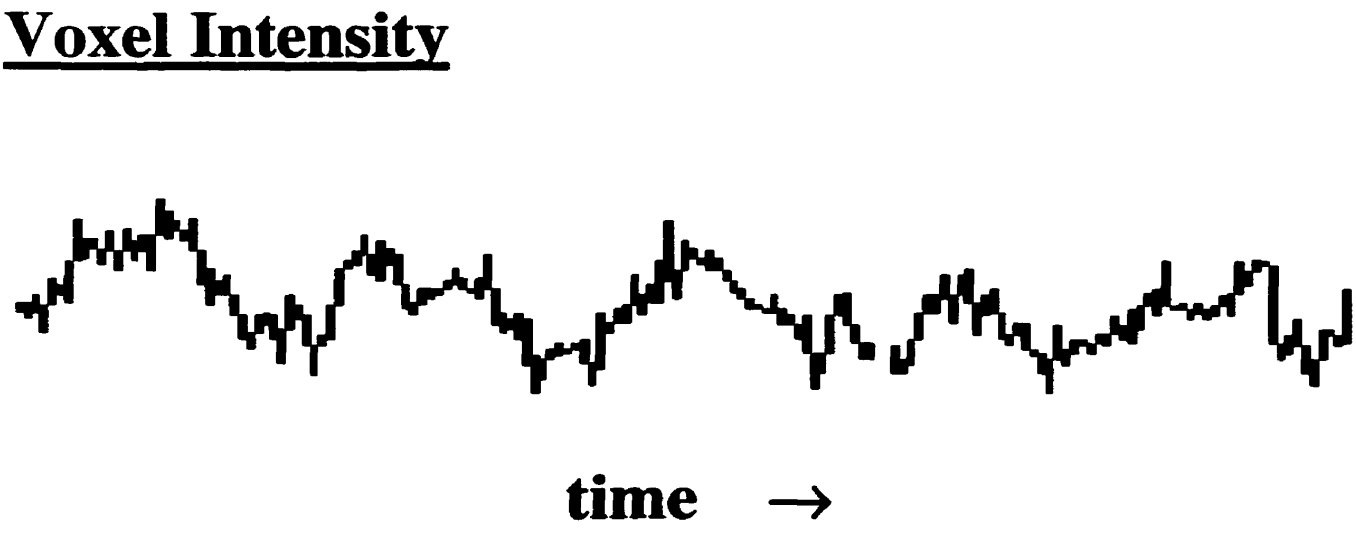

Figure 1.4. In blocked experimental design, the voxel signal intensity versus time often resembles the shape of the idealized task waveform. This similarity motivates the use of correlation analysis to produce functional images.

where f_i is the intensity of the voxel in the i^{th} image, r_i is the reference waveform, and μ_f and μ_r are the average values of f and r, respectively.

The correlation coefficient, however, only characterizes the similarity of the waveform shapes, and gives no information concerning the amplitude. A weighting factor, a ratio of relative change of activation intensity with respect to the reference waveform, is applied to the correlation coefficient to express relative amplitude information. Activated voxels are then usually color-coded corresponding to the relative amplitude of the change in signal intensity and overlaid on top of an MR anatomical image acquired during the same fMRI session. Figure 1.5 shows an example of an fMRI scan of a healthy young adult performing a blocked design right-handed finger-tapping task. As expected, activation of the contralateral primary motor cortex is indicated.

1.2 Head Motion and Image Artifacts

Even very slight subject motion can lead to false positive and false negative regions of activation because the small BOLD effect can be easily missed if the signal intensity of the "snap-shot" images is corrupted by significant head movement. Severe activation artifacts can result and image data must often be discarded. For instance, an fMRI study investigating primary motor cortex localization in brain tumor patients discarded 5 out of 17 patients' data due to gross head motion during the scans, even though foam padding was used to help stabilize the subject's head [23]. It has been found that 30-90% of fMRI signal variance can be attributed to motion [24].

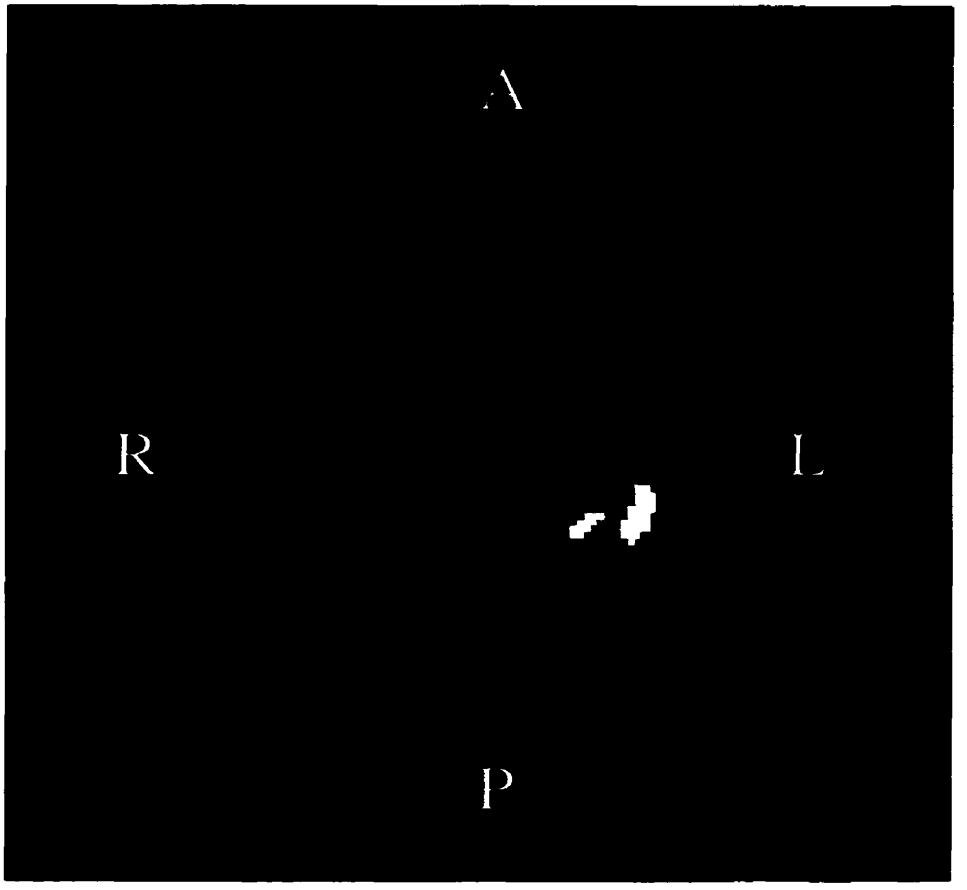

Figure 1.5. Functional image of right-handed finger-tapping for a young healthy adult. White pixels show left-hemisphere primary motor cortex activation (blocked design: 30 s tapping/30 s rest; 5 repeats). [R=right, L=left, A=anterior, P=posterior]

fMRI: Spiral, TR=1500 ms, TE=40 ms, flip angle= 80°, 7 mm slice, 9 slices, 64x64 matrix, FOV=20 cm, threshold: $p<0.05$
Anatomical MRI: 3D T1 weighted gradient echo imaging, TR=15 ms, TE=3.4 ms, flip angle=35°, 1.2 mm slice, 124 slices, 256x192 matrix, FOV=22 cm

Subject head movement also leads to decreased resolution of fMRI scans. If head motion is random and only causes blurring of the images, the effective full width half maximum (FWHM) of a functional MR image is defined as:

$$FWHM_{effective} = \sqrt{FWHM_{movement}^2 + FWHM_{scanner}^2} \qquad [1.6]$$

where $FWHM_{movement}$ is FWHM of the head motion, and $FWHM_{scanner}$ is the spatial resolution of imaging system. If the subject's head motion is greater than the resolution of the imaging system, then the effective resolution is closer to that of the head motion [25, 26].

The two general types of movements are physiological fluctuations (breathing, cardiac pulsation, swallowing) and gross head motions produced by the inability of subjects to keep their heads perfectly still. The latter usually predominates, gets worse throughout the fMRI examination, and often manifests as task-correlated motion, which leads to false positive activation [27]. Task-correlated motion arises when the subject's head moves in synchrony with the task pattern (*eg* the head translating at the start of each task period and returning back to the original position at the end of each task interval). The result is often a characteristic ring of false activation around the head, because of the large signal intensity difference between air (zero signal) and the head's boundary. Such rings are also observed in regions of signal loss within the brain due to magnetic field distortion near other air/tissue interfaces, such as brain sinuses, also due to the large signal intensity differences at the interface. It is clear, however, that activation deep within the brain is also affected by task-correlated motion. It has been suggested that if the activation between two groups of subjects (e.g. healthy volunteers and patients) is to be compared, the possibility of a group difference

in task-correlated motion must be excluded before considering other interpretations of any observed differences [28].

Head motions are also augmented by random shifts in the subject's posture (either as a slow drift or rapid movement). The simple act of breathing can also lead to direct movement of the subject's head [29]. The beating heart's influence on brain vasculature can cause the brain and cerebral spinal fluid to pulsate [30]. Techniques to reduce or eliminate these physiologically induced artifacts in MR images are being investigated [31, 32].

Functional MR images can also be degraded by movement far away from the brain, especially if the motion's periodicity is the same as the block design [33]. Swallowing or speaking not only leads to motion of the head, but to magnetic field disturbances in the region of the brain [34]. Although these artifacts are not induced by head motion, they pose a severe problem to fMRI, especially in areas close to bone to air interfaces.

1.3 Current Interimage Motion Correction Techniques

Motion artifacts can be classified as intraimage (within the same image) and interimage (between different images in a time series). Intraimage motion artifacts are adequately minimized using "snap-shot" imaging. Interimage artifacts pose the more severe problem, as described above. Numerous methods of motion minimization and correction are being developed and studied to combat interimage artifacts. There are three general strategies currently under investigation: 1) head restraint; 2) retrospective motion compensation; and 3) prospective (real-time) correction methods. Of these strategies, the first two are more established and often significantly reduce motion artifacts, but are frequently an incomplete

solution even when used in combination. The use of real-time correction methods still remains largely unexplored.

1.3.1 Restraints

A variety of restraining devices have been investigated to attempt head immobilization during fMRI. A very simple, inexpensive standard method is to pack foam padding between the head and the MR head coil, but this is often insufficient [23]. An alternative is a vacuum pillow, consisting of a plastic bag filled with small plastic beads that mold around the subject's head once the air is evacuated from the bag. The vacuum pillow is relatively comfortable and easy to use, but is not a sufficiently rigid restraint and is quite bulky. Another type of head restraint is a thermoplastic mask. A thermoplastic mask consists of a sheet that, when heated with a warm water bath, can be placed on the subject's face to form a mold. After cooling, the mask is fixed to the scanner table to immobilize the subject. They have been shown to be effective in relaxed and cooperative subjects in a PET study [35]. This technique does not provide complete restraint, and can potentially introduce water into the magnet bore (in addition to wetting the patient's head). More restrictive clamping systems can be used, but these can actually increase head motion because of discomfort from pressure points on the scalp. Subjects tend to move to alleviate the pain, which can result in another painful pressure point [25].

Bite bars (a subject bites down on an immobilized, individualized dental mold during fMRI) have been utilized with good results. As can be imagined, such devices can be uncomfortable and tiring, especially considering that an fMRI session can be more than an hour. Bite bars can also be contraindicated for clinical use because there can be a need to

disconnect the restraint systems quickly [25] and can stimulate the gagging reflex [36].

Some of these stabilization methods can be used concurrently. For example, hard foam wedges inserted between the subject's head and a modified football helmet fixed to the MR table was adequate for "highly motivated subjects from the investigators' research group", but the use of a bite bar was necessary for other volunteers [37]. A thermoplastic face mask and bite bar were used for a PET study, but the dental mold was only used periodically for positional measurements and then removed for better comfort [36].

In the extreme case, stereotactic fixation can be used on a small subset of subjects who have their heads immobilized in preparation for brain surgery, which obviously results in very little head motion during fMRI [38]. The stereotactic frame, however, must be compatible with the MRI scanner.

1.3.2 Retrospective Techniques

Many different retrospective techniques are being used and investigated for head motion correction, but none of them completely solve the problem. Comparative studies of all these techniques have not been fully performed, and their use is widely variable. It is, therefore, often difficult to compare results from different fMRI studies.

Image coregistration is the predominant method to correct for head motion retrospectively. There are many different techniques to align images acquired in a time series to compensate for gross head motion [25]. A well-known algorithm was developed by Woods et al. [39] and is included in the AIR (Automated Image Registration) package. This technique minimizes the variance of the signal intensity ratio of two image volumes (the target ratio for perfect alignment is unity, with zero variance) by varying the 3 translational

and 3 rotational degrees of freedom.

There are alternatives to purely intensity-based techniques. Through-plane motion and temporal inhomogeneities of the magnetic field can also bring new, previously unexcited protons into the imaging plane, altering the signal intensity and, thus, confounding intensity-based realignment. In a comparison of intensity-based coregistration with a method based on image contours, the latter was judged superior and less sensitive to the signal intensity changes from through-plane motion and temporal magnetic field inhomogeneities [40]. Intensity-based coregistration remains widely used, however. Other alternatives involve the use of reference scans for coregistration and voxel signal intensity correction based on coregistration estimates, to improve assessment of through-plane motion [24]; investigating different interpolation effects in the reslicing of the volume of interest [41]; and registration of individual slices instead of an entire volume (slice-stack approach) into an anatomical volume [42]. If gross head motion occurs during the fMRI scan, each "snap-shot" image will have experienced a different amount of motion because each slice was taken consecutively rather than simultaneously [42]. Head motion can also be monitored during the scan and then used later for motion correction, as shown using emission computed tomography [43].

There are also numerous approaches to correct the artifacts caused in fMRI by respiration and the beating heart. Physiological fluctuations can be estimated and corrected retrospectively by monitoring breathing and heart beat during fMRI acquisition [44]. An alternative to external physiological monitoring is direct retrospective extraction of physiological activity from the MR data [45]. This approach eliminates the risk of disturbing the magnetic field with monitoring equipment, and extra apparatus is not needed. K-space phase variation maps can be used to show cyclic phase variations due to breathing and heart

beating. This information can then be used to perform k-space correction [46]. Functional MRI data can also be digitally filtered to suppress cardiac and respiratory structured noise by defining regions of the image where neural activation is unlikely and determining the time series of the noise sources. The time series can then be used to filter the noise patterns from the regions of the brain where activation is expected [47]. Filtering techniques can be useful in situations where there is no aliasing (*ie* "snap-shot" images sample the motion adequately quickly to determine the true frequency) and no large transient head movements.

1.3.3 Prospective Techniques

Prospective motion correction techniques are starting to receive attention. Such methods are attractive because, unlike retrospective methods, they enable determination of the quality of fMRI data while the subject is in the scanner. They enable the current time series to be terminated if there is too much motion. The subject can then receive further training and instruction, and the fMRI data collection can be repeated. This approach makes better use of both scan time and subjects.

The simplest prospective approach involves the development of near real-time statistical analysis of fMRI data using recursive algorithms, yielding preliminary activation images that enable the behavioural task to be controlled, altered, or repeated depending on physiological monitoring and motion behaviour [48, 49]. Real-time 3D image coregistration is also now possible [50, 51]. A second level of complexity involves the prospective manipulation of MR pulse sequences for correcting head motion. For instance, spatially localized RF excitation can be used prior to taking the fast images to suppress physiological eye movement artifacts instead of trying to correct retrospectively for it [52]. Several other methods have

been developed to enable the imaging scan plane to track with head motion [53, 54, 55, 56, 57]. These methods all require a reliable method to measure head motion quantitatively. An area of active investigation is in the use of "navigator (NAV) echoes". Each NAV echo provides a one-dimensional projection of the object being imaged. Displacements of the object can be determined by cross correlation of the projection with a reference projection. Successive NAV echoes, therefore, enable tracking of the translational motion along one axis. Using orthogonal NAV echoes, displacements in more than one direction can be determined [58, 59]. Alternatively, "orbital" navigator (ONAV) echoes (data points acquired along a circular trajectory in k-space) are more efficient and can be used to measure rigid body in-plane rotational and translational motion simultaneously, through shifts in the magnitude and phase of successive echoes, respectively. In real-time correction, an ONAV echo is performed before each fMRI "snap-shot" image is taken [60, 61]. Based on the ONAV echo data, the imaging plane can then be adjusted to track the head motion. It has been found that one dimensional translational NAV echo fMRI motion correction can be performed in 100ms with 0.5 mm sensitivity [53], and through-plane and in-plane inter-image head rotation correction for fMRI has been demonstrated [54]. Very recent studies have used multiple ONAV echoes to perform simultaneous multiaxial motion detection [62].

Although this technique is promising, ONAV echoes suffer from several limitations. The extra time necessary for ONAV echoes inevitably reduces the maximum number of slices that can be acquired per TR interval, which has implications for temporal resolution. It has also been suggested that ONAV echo data could "not, in our experience, change in such a way as to provide reliable measurement of rotational motion" [56]. Another disadvantage is that the acquisition of ONAV echoes makes it impossible to measure brain activation within

the region of magnetization from which the ONAV echo is formed. The use of ONAV echoes can also be complicated and time consuming for measuring motion with all six degrees of freedom (three rotation angles, three translations) because 3 ONAV echoes are necessary.

Other real-time tracking techniques have been proposed that use MR-based position measurements, such as use of fiducial markers, spatial-frequency tuned markers (samples that act as MR-visible markers when observed with NAV echoes [56] or receiver coils containing small marker samples [55, 57]). For complete determination of the translational and rotational movement of a rigid body, at least 3 markers are necessary. The receiver coil method is less practical because each of the coils can affect the signal that the other coils are receiving. Head position measurement is also possible using other tracking equipment, which then must communicate with the scanner to enable scan plane adjustment according to the position measurement data. One such device uses 3 semiconductor lasers and 3 position-sensitive detectors (PSDs), each with a linear accuracy of better than 100 microns in the direction of light propagation [63]. The laser light bounces off 3 reflectors attached to the subject's head and is detected by the PSDs. Alignment of the lasers and PSDs, unfortunately, can be very difficult. Studies using this system are still preliminary, and the position accuracy for 6 degrees of freedom tracking remains to be determined. Success has been reported for prospective scan plane alteration to track the same anatomical plane after head movement via the head motion information gained from prospective coregistration [64].

Lastly, behavioural feedback during the scan via MRI compatible tracking systems can be used to compensate prospectively for head movement [25, 65]. By viewing a representation of his/her head motion data, the subject can subsequently alter his/her

behaviour to try to reduce the amount of motion. This could work well with alert and cooperative subjects, but would not be helpful for others, such as stroke patients with diminished cognitive capabilities. Furthermore, it alters the behavioural task that is being assessed.

1.4 Characterizing Head Motion

Given the large amount of attention devoted to reducing motion artifacts in fMRI, there is surprisingly little quantitative data describing the actual characteristics of subject head motion during fMRI. This information is critically important to the effective design of restraints, retrospective, and prospective motion correction techniques. Several PET studies, however, have been performed to investigate the head motion characteristics of young healthy subjects. The results give an indication of the severity of head motion during imaging. For example, it was found that during a 130 minute PET scan, head rotations in the sagittal and coronal planes were up to 4.1 and 2.4 degrees respectively [36].

During another PET study, cooperative and relaxed subjects wore thermoplastic masks. Their head movements were 3-10 mm in all three translational directions during one hour. Long periods of minimal head motion followed by abrupt translation or rotation in multiple dimensions occurred. It was also observed that head movement increased with scanning duration even when using a thermoplastic mask, but that the rate and magnitude of increase were much smaller than when no restraint was used. It was concluded from this study that thermoplastic masks could be suitable for PET or SPECT imaging but perhaps are not sufficient for fMRI because of its higher resolution. It was further suggested that the time

necessary for molding and cooling of the thermoplastic masks could be too long for routine clinical use [25, 35].

To investigate head motion during frameless stereotactic radiosurgery, a study monitored the head movement of cooperative young healthy subjects [66]. Nearly all cumulative standard deviation values of motion increased with study length. It was also found that when the standard deviations of independent 5 minute data segments were determined, they were small and nearly constant throughout the study period. These two observations suggest that there are low frequency trends in head motion with constant higher frequency head movements superimposed. Further findings include that the standard deviation values in the z-direction (head to feet direction) were larger than those in the x and y directions, with maximum amplitude of 1.44 mm when the subjects were not restrained. The increased standard deviation in the z-direction was attributed to the effect of swallowing.

Much less is known about the head movement behaviour during imaging of people who are not young and healthy volunteers, such as the elderly and patients. The few studies that have been performed with these groups have indicated that head motion is often significantly different. For example, the head motion of elderly volunteers to that of young subjects were compared during an fMRI study. It was found that the head motion of the elderly group was much larger than that of the young group [67]. Different characteristics of head motion in patient populations were illustrated in a study that showed that schizophrenic subjects have more task-correlated motion than controls when using a silent verbal fluency task during fMRI. It was found that the head motion of the control group was dominated by linear trends, while schizophrenic subjects' head motion had more task-correlated rotations [28].

1.5 Motivation behind Study

1.5.1 Why Characterize Head Motion Further?

Head movement characterization clearly can be considered an important element in the design of motion correction methods for fMRI. By determining the extent and frequency of head motion, optimal real-time tracking equipment and more efficient prospective and retrospective correction algorithms can be developed and exploited. Head restraint designs can also be optimized for comfort and immobilization if the amount, direction and type of motion (translational and rotational) are determined *a priori*. For example, if head motion occurs mainly in one rotational direction, the restraint could limit movement only in that orientation, leading to a more open and comfortable restraint. Characterizing head motion in different groups of subjects is also of great significance to eliminate false assumptions that head motion of unlike populations is similar.

1.5.2 Head Motion and Stroke Patients

In this thesis, the population of interest has been chosen as patients recovering from stroke. Stroke is the third most common cause of death in the majority of Western countries and the primary cause of chronic adult disability. It is an extremely costly disease in terms of direct (hospitals, physicians, drugs, research) and indirect (premature death, short and long term disability) expenses, totaling $2.8 billion in Canada for 1993 [68]. Stroke incidence increases with age. Although age-specific rates appear to be decreasing, the incidence of strokes could increase because of the aging population. Women have a higher lifetime risk than men, which is attributed to the fact that women in general live longer.

Stroke is often a debilitating disease. Effects vary and commonly include hemiparesis

(paralysis/weakness of one side of the body), aphasia (language difficulties), dysarthria (slurring of speech), memory challenges, and personality changes. Recovery of lost function post-stroke is through a complex, individually variable, and poorly understood reorganization of the brain [69, 70].

Of particular interest in understanding stroke recovery is reorganization of brain regions involved in motor function (hand and leg) because of the prevalence of hemiparesis after stroke and the importance of motor function for patient independence and quality of life [70]. When the primary motor system is affected, there is re-weighting of the brain activity for motor function between various areas, such as to the primary motor cortex in the opposite hemisphere and secondary motor regions [71]. Hand motor (*eg* finger tapping and hand gripping) functional studies can often be performed successfully with patients recovering from stroke. For example, it was found during an fMRI study using a finger-tapping task that stroke patients activated the same regions of the brain as the controls but to a larger extent, particularly in the unaffected hemisphere [72].

Unfortunately, motor tasks can also cause severe motion to be translated to the head during fMRI, because stroke patients often recruit proximal limb muscles during attempted distal muscle motor tasks. Figure 1.6 is an example of a motion-corrupted functional MR image of a stroke subject performing right-handed finger tapping. Although this problem often occurs during finger tapping tasks, performing foot motor tasks during fMRI are thought to result in even more motion translation to the head. Foot recovery is of great interest, however, because it is necessary for ambulation of the stroke patient with hemiparesis.

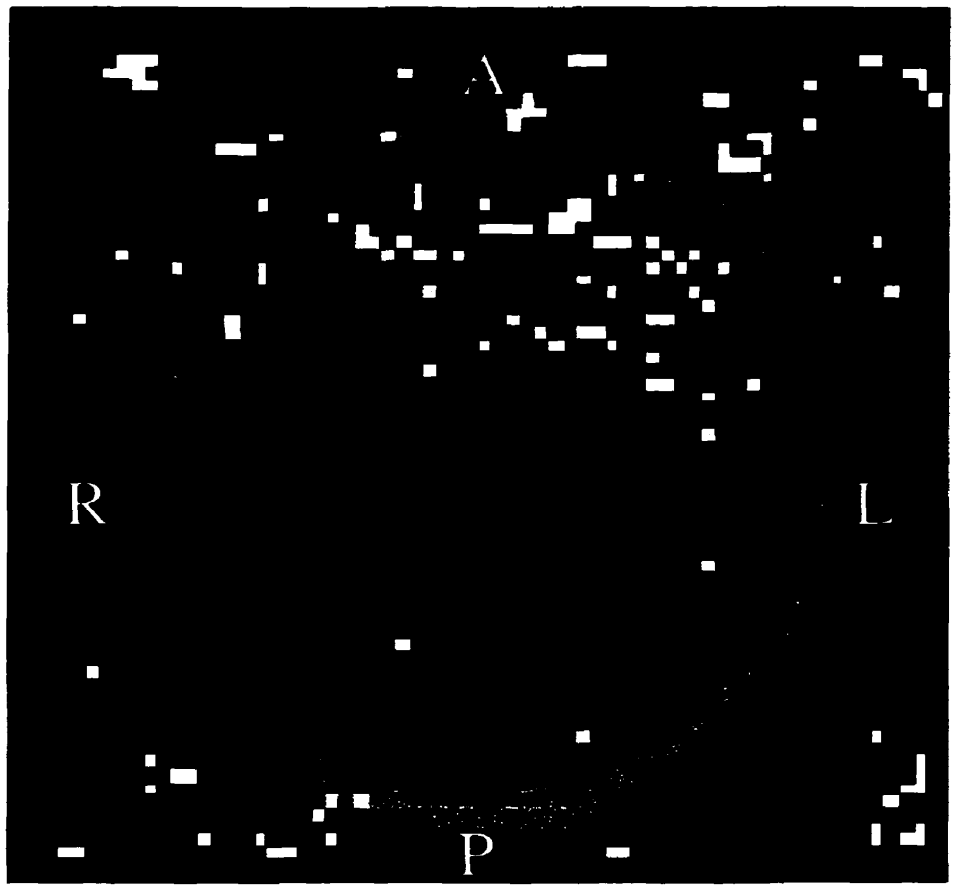

Figure 1.6. **Functional image of right-handed finger-tapping for a stroke subject, showing false positive activation due to head motion (task design, imaging parameters, and activation threshold identical to that of Fig. 1.5).**

1.5.3 Why are MR Simulators Useful?

The advantages of simulators in fMRI research are underappreciated, yet particularly relevant to this thesis. In conjunction with a position-tracking system, a simulator provides a fourth method of head motion reduction, namely training and screening of subjects. Using MR scanner time for subject training is costly and impractical. An MR simulator presents a less intimidating introduction to a real MR scanner. It allows a more relaxed atmosphere with almost no time constraints to vacate the vicinity of highly utilized equipment. It also provides an opportunity to have "dry runs" of new fMRI protocols and set-ups, to train subjects to perform tasks correctly.

As mentioned previously, some subjects are unsuitable for fMRI because they cannot remain still due to claustrophobia and anxiety, or poor head control. People who are deemed inappropriate subjects for an fMRI scan, even after habituation to the simulator and practice of the task, can be screened out using a simulator. Training sessions with an MR simulator decrease the anxiety level of children compared to those without a training session and might be able to replace sedation of the children [73]. There is, therefore, strong motivation to conduct experiments to characterize head motion produced during behavioural tasks in simulators, where task monitoring and position tracking are greatly facilitated.

1.6 Hypothesis Statement

Head motion characterization is an important factor for designing strategies to improve the quality of fMRI data. Specific objectives associated with this hypothesis are:

1. To characterize head motion during fMRI motor tasks (*eg* dominant directions of motion)

2. To investigate whether:

    - groups (young controls, age-matched controls, stroke patients) exhibit different head motion characteristics
    - tasks and restraints result in different head motion characteristics

3. To investigate the potential of MR scanner simulators for improving fMRI methodology

The experimental approach to addressing these objectives, the data obtained, and the ramifications of these results are discussed in the following two chapters.

Chapter 2

Quantifying Head Motion Associated with fMRI Motor Tasks

by E. Seto, G. Sela, W.E. McIlroy, S.E. Black, W.R. Staines, M.J. Bronskill, A.R. McIntosh, S.J. Graham

A paper submitted to Neuroimage, September, 2000

2.1 Introduction

As described in Chapter 1, fMRI is a powerful tool in neuroscience research [1, 2, 3, 4]. The technique is comparatively new, however, and is not without methodological deficiencies that limit clinical applications. In particular, head motion is a frequent problem in fMRI due to long examination times (typically multiple fMRI scans of several minutes within a session of approximately 1 hour), and the small signal changes from the BOLD effect ($\approx 4\%$), leading to false positive and false negative inference of neuronal activation [24, 27, 28]. The use of motor tasks, a major avenue of research, compounds the problem because the motion associated with the task (*eg* finger tapping) can translate to the head. Methods to minimize and correct for head motion using restraints [25, 35, 36, 37], fast imaging [17, 19, 20], and retrospective image processing [24, 25, 40, 41] are currently used in combination, but do not always provide sufficient compensation. In this situation, fMRI data are often discarded [23].

A small amount of quantitative literature exists on head motion of healthy young adult volunteers, mainly in the context of PET [25, 35, 36]. Many patient populations, particularly those with motor control difficulties, such as stroke patients, will likely exhibit head motion greater than that of young healthy adults [28]. The extent of this problem in patients warrants investigation. Considering that fMRI of certain patient populations is particularly challenging due to head motion, quantifying head motion in these populations could be useful in designing strategies for improving the clinical robustness of fMRI.

The head motion characteristics of stroke subjects during simple motor tasks were investigated, compared, and interpreted with respect to those of age-matched controls and young healthy adults. These particular subject groups were chosen because understanding stroke recovery mechanisms [69, 70, 71] and changes in brain function with normal aging [67] are active areas of fMRI research. Head motions from hand gripping and foot flexing tasks were compared to determine whether foot motor tasks introduce an unacceptably large amount of motion to preclude fMRI studies investigating stroke recovery of the lower limb. Different conditions (*eg* use of restraints) were also examined to assess effectiveness. Measurements were performed with a highly accurate infrared tracking system under simulated fMRI conditions.

2.2 Methods

2.2.1 Subjects

Six stroke subjects (3 females and 3 males, average age: 58, range: 22-78) that represented the population of interest for fMRI motor recovery research were recruited.

Selection criteria included moderate to severe motor impairment on one side of the body (hemiparesis) gauged through the Chedoke-McMaster Stroke Assessment-Impairment Inventory (scored 2-5 on a scale between 1-7, 7 being normal) [74], and the ability to lie reasonably still for several minutes. The Chedoke-McMaster criterion permitted rejection of stroke patients who could not perform the necessary fMRI motor tasks (low score), and those with recovered motor function whose ability to remain still would not be a particular concern (high score). Seven control subjects age-matched to the stroke subjects (5 females and 2 males, average age: 59, range: 25-71), and 10 young healthy adults (4 females and 6 males, average age: 28, range: 25-38) were also recruited for comparison.

2.2.2 Tasks

Subjects performed hand gripping and foot flexion motor tasks according to Table 2.1. Each task was performed at approximately 0.5 Hz, depending on the subject's capability, for 15 seconds followed by 15 seconds of rest. This cycle was repeated, such that each trial in the experiment lasted 1 minute. The start of the task and rest phases was verbally cued.

The motor tasks were chosen for three reasons: 1) the importance of unilateral and bilateral hand gripping for the fMRI study of hemiparesis and extinction during stroke recovery [75], 2) to investigate the effects of restraining the moving limb, and 3) to investigate the potential benefit of a foot flexion device designed to translate the foot flexion motion to the free floating knee instead of the head. The foot flexion device was a wooden apparatus with two plastic strips. The subject's foot presses against a pivoting pedal, allowing the ankle to rotate. To keep the foot in place, a velcro strap was attached to the

Task	Restraint
Unilateral (affected side) hand gripping	None
Bilateral hand gripping	None
Unilateral hand gripping	Forearm restraint
Unilateral (affected side) foot flexion	None
Bilateral foot flexion	None
Unilateral foot flexion	Pelvic restraint

Table 2.1. Motor tasks used for this study.

subject's calf, binding the two plastic strips against the calf. Another velcro strap was used to keep the foot from slipping off the pedal (Fig.2.1a).

As a measure of each subject's compliance during the tasks, foot flexion was monitored with a fiber-optic Shape Sensor™, (Measurand, Fredericton, New Brunswick) and associated software. The 10 cm active region of the fiber, located near the tip of the optical fiber, was strapped to the center of the front of the foot that bends during dorsi and plantar flexion (Fig. 2.1a). Hand gripping was monitored using force sensing resistors (FSR's) mounted on the outside surface of two hollow plastic cylinders (Fig. 2.1b). The force waveform was recorded via a laptop computer running Labview software (National Instruments, Austin, Texas). Equipment availability allowed collection of hand gripping data for 5 age-matched controls and 4 stroke subjects, and foot flexion data for 6 age-matched controls and 2 stroke subjects.

2.2.3 Experimental Set-up

2.2.3.1 MR Scanner Simulator

The MR scanner simulator (Fig. 2.2 and 2.3) consisted of a hospital gurney lined with a thin foam sheet. A surplus GE Signa head coil was mounted to the gurney and a vacuum pillow (VacFix Systems Inc., Odense, Denmark) was used to stabilize the head. A thin sheet of plastic arched over the subject created a tunnel (60 cm across, 40 cm high, 122 cm long) with bore dimensions similar to those of the GE 1.5 T Signa MRI scanner (CV/i, V8.25). Limb restraints, when used, were fastened by velcro to each side of the MR simulator bed. The subject's legs, supported with a pillow under the knees at all times, were elevated

a)

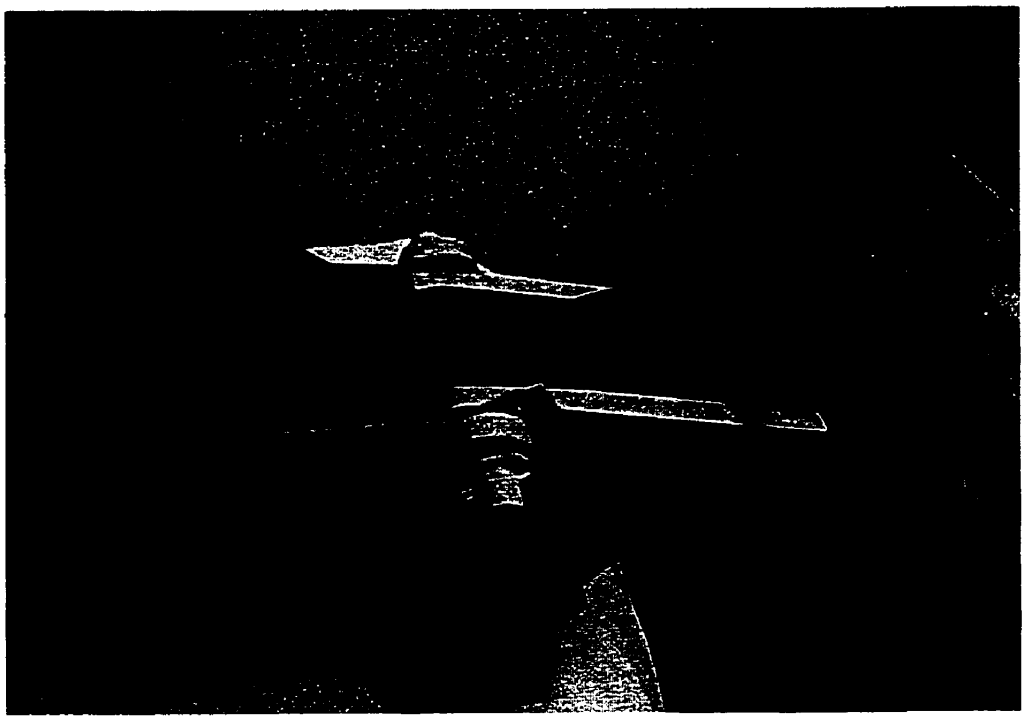

b)

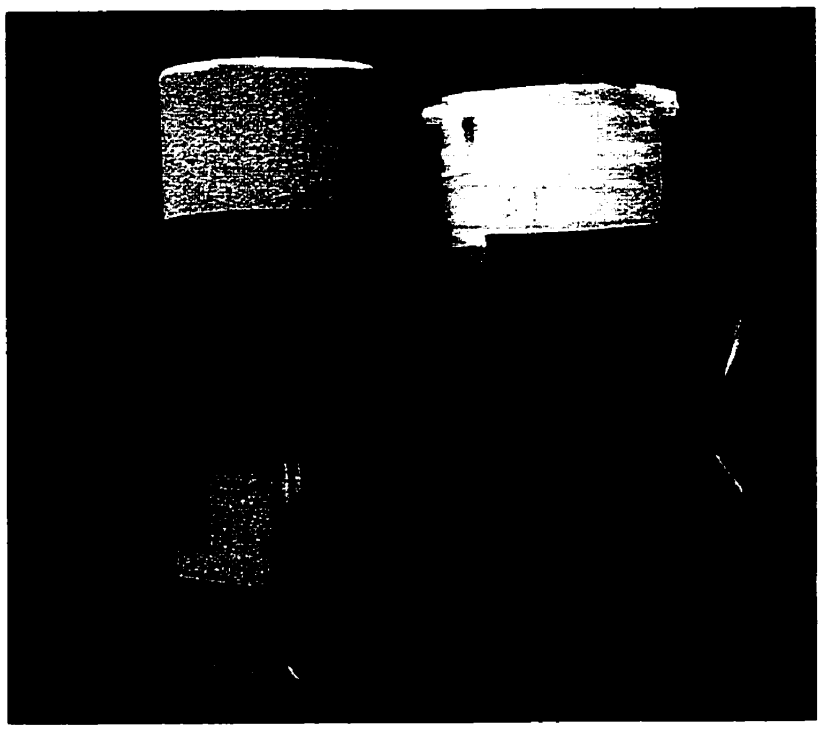

Figure 2.1. (a) Foot flexion device and Shape Sensor™ optical fiber attached to the anterior section of the ankle to measure the amount of bend during foot flexing task. (b) Hand grips made from plastic pipes. Force sensing resistors (FSRs) are attached to the surface of each pipe to monitor subject compliance during hand gripping tasks.

a)

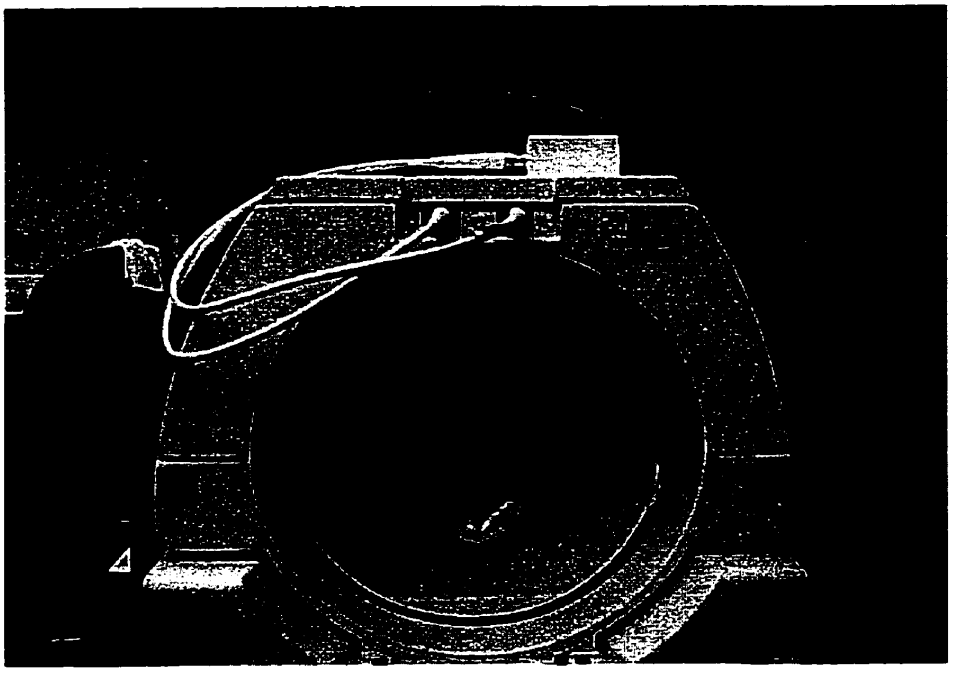

b)

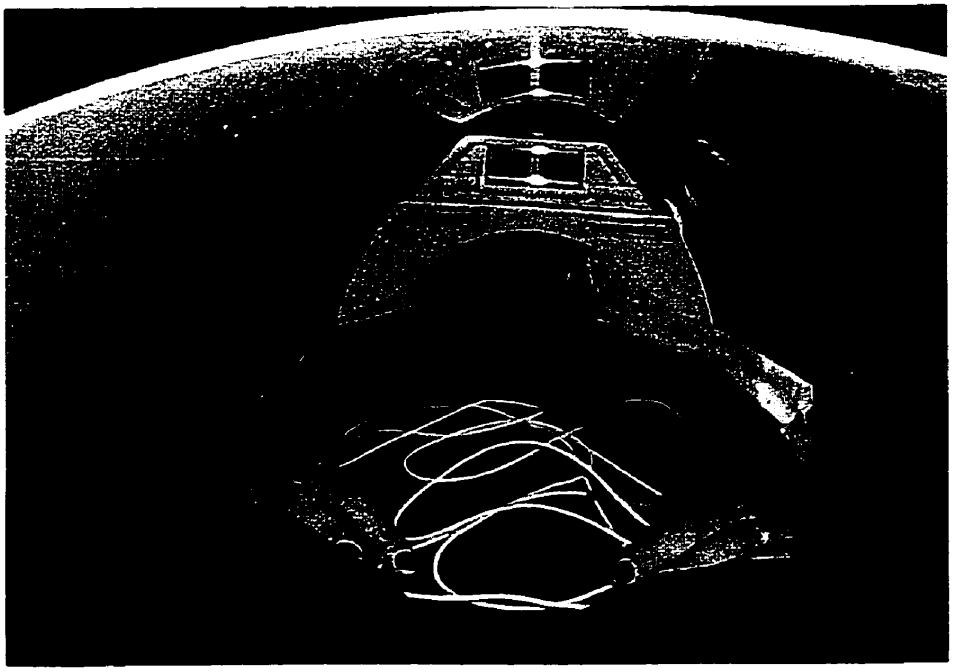

Figure 2.2. Subject in simulator; view from Polaris camera of cap with attached Polaris tool and vacuum pillow (a) and view inside simulator (b).

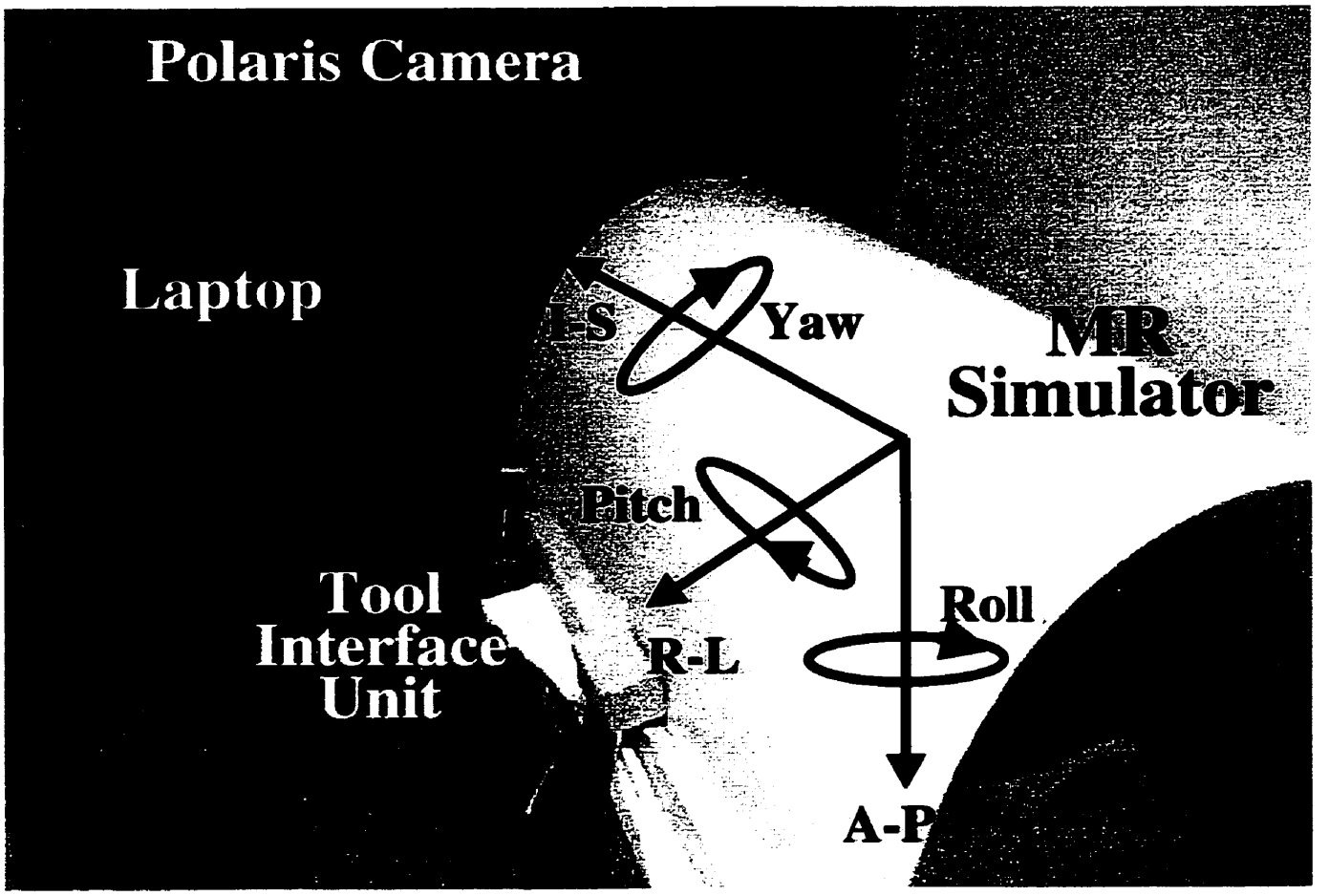

Figure 2.3. Experimental set-up showing MR simulator and Polaris Tracking System (co-ordinate system also indicated, A-P: anterior-posterior, R-L: right-left, I-S: inferior-superior).

sufficiently such that the heels of the feet were not touching the bed during the foot flexing tasks.

2.2.3.2 *Polaris Tracking System and Initial Evaluation*

Head motion was measured using an active Polaris tracking system (Northern Digital Inc., Waterloo, Ontario). Two separate charge-coupled devices (CCDs) built into the camera unit detected infra-red light from at least three of the 12 infra-red emitting diodes (IRED's) contained in a specially constructed tracking tool with precisely defined geometry (Traxtal Technologies Inc., Toronto, Ontario). The six degrees of freedom (3 orthogonal translation directions and 3 rotations) of the tool were determined based on parallax. The tool was fixed to the subject's head using a specially designed cap prior to positioning the subject supine in the simulator. The top of the subject's head faced the Polaris camera through the bore of the simulator (Fig 2.2). The positional information was recorded onto a laptop computer using an RS232 interface. Figure 2.3 displays the entire experimental set-up and the co-ordinate system used throughout this chapter.

The accuracy and stability of the Polaris system were determined prior to measuring the subjects' head movement, over the range of motion ($\approx$1 cm) expected in this study. To test the tracking accuracy, the Polaris tool was tightly clamped onto a stage capable of translating in 3 orthogonal directions (accurate to 0.002 mm) and rotating in 2 orthogonal orientations (accurate to 0.2° for roll and 0.4° for pitch). Both the stage and the Polaris camera were fixed to an optical bench. By conducting multiple repeated measurements of the stage at precise angular and position increments over a 1.5 cm diameter volume, the anterior-posterior (A-P) and right-left (R-L) accuracy (root mean square error between true and

measured positions) were found to be 0.03 mm, while the inferior-superior (I-S) direction had an accuracy of 0.12 mm, which was anticipated to be greater due to parallax. The angular accuracy in pitch and roll was 0.23° and 0.09° respectively. All accuracy measurements were much smaller than the expected head motion.

To determine the stability of the Polaris system, the position of a stationary object was recorded as a function of time from when the system was turned on to 1.5 hours. The resulting measurements drifted significantly (up to 1 mm), as the camera warmed up. Importantly, the drift leveled out after about half an hour and the short-term (1.5 minutes) stability of the Polaris system was much less than 0.1 mm even during the largest drift rate (immediately when the system was turned on). The stability of the system therefore sufficed for this study. To achieve maximal stability, the Polaris system was warmed up for at least 1 hour prior to use.

To assess the validity of using the simulator by comparing head motion data from subjects inside the simulator and inside the MR scanner, the compatibility of the Polaris system with the MR scanner's high magnetic field was first tested. The camera unit was found to function properly in the magnetic field once the unit's power supply was located outside the magnet room with the appropriate cabling. The Polaris Tool Interface Unit (TIU) and the laptop were similarly located outside of the MR scanner room. A wooden frame was constructed such that the Polaris camera straddled the patient table track at the back of the MR scanner, providing direct line-of-sight to the top of the subject's head. The camera was positioned at approximately the same distance and orientation from the tool as achieved with the simulator system.

The head motion of the 10 young control subjects was measured both inside the simulator and the MR scanner for all 6 tasks. Measurements were performed at 6 Hz (167 ms sampling period, ensuring that 9 data samples were acquired within 1.5 s, the typical time scale of repeated "snap-shot" image acquisition of the same slice during fMRI of the whole brain). The Polaris system, however, can acquire data at a maximum rate of 60 Hz (≈2 data samples per 40 ms k-space readout).

2.2.4 Analyses

Three different metrics were used to interpret the head motion data: 1) the sample standard deviation of the head motion (with linear trends first subtracted) (M_{sd}); 2) the cumulative motion (the sum of all the distances between each position measurement over time) (M_c); and 3) the range of the head motion (M_r). The metric M_{sd} is described by the formula:

$$M_{sd} = \sqrt{\frac{\sum_{i=1}^{N} (X_i - \overline{X})^2}{N-1}} \qquad [2.1]$$

where X_i is the head position measurement at a particular time i, $\overline{X}$ is the mean of all the head position measurements, and N is the total number of data points. M_c was calculated as follows:

$$M_c = \sum_{i=1}^{N-1} | X_i - X_{i+1} | \qquad [2.2]$$

M_r is described as:

$$M_r = X_{max} - X_{min} \qquad [2.3]$$

where X_{max} was the maximum and X_{min} was the minimum head position measurement. The metrics were calculated separately for both task and rest conditions.

These metrics were applied to the 3 translational and 3 rotational directions of the head. Unless the direction of head movement was being examined, the three degrees of translation (anterior-posterior, superior-inferior, and right-left) were added in quadrature to provide a single distance measurement to facilitate data interpretation prior to application of the metrics. The main focus was directed at M_{sd} because of the obvious physical meaning. M_c was a cruder confirmation of whether head motion increased or decreased during different tasks. M_r indicated the severity of the transient head motion, with the proviso that an unusually large twitch could skew the results and not fairly represent the general head movement.

Statistical analyses were performed using SPSS (Statistical Package for the Social Sciences, version 10.0, Chicago, Illinois). A repeated measures 2-way analysis of variance (2-way RANOVA) of the subject groups and four out of the six tasks (unilateral hand gripping, unilateral hand gripping with restraint, foot flexing with device, and foot flexing

with device and restraint) was performed for all three metrics, to determine group differences, task differences, and interactions between the groups and tasks (*ie* whether task differences depend on group). M_{sd} and M_c values used for the analyses were the average of the two task periods for each subject. M_r values used were the larger of the two ranges of the task periods for each subject (rest periods were ignored).

Other analyses included a comparison of task-correlated motion by a 3-way RANOVA of the subject groups; task vs. rest periods; and the unilateral hand gripping without restraint vs. foot flexing with the foot device but no restraint. The mean head positions during the task and rest periods were also examined to determine if there was a positional shift during the transition between task and rest. Directional dominance was analyzed separately for translation and rotation of the head during the unilateral hand gripping without restraint and foot flexing with the foot device but no restraint through four 2-way RANOVA's of the subject groups and directions. The question of how bilateral vs. unilateral hand gripping affected head motion was examined by a 2-way RANOVA of the subject groups and the unilateral and bilateral hand gripping data. Repeated measures t-tests were also performed to determine for which group there were head motion differences during unilateral and bilateral hand gripping. Finally, the effect of the foot device on head motion was determined by the analogous assessment procedure used for the unilateral vs. bilateral hand gripping data.

The variance in the amount of head motion between the subjects from the three groups was often significantly different (at least a multiple of 4), with the largest variance observed in the stroke subject group and the smallest variance observed in the young controls. Where indicated, a square root transformation was first applied to bring the

variances of the groups closer together to allow parametric testing. This transformation is often used when the variance increases as the mean increases, as was observed in this study.

2.3 Results

2.3.1 Initial Observations

The subjects in all three groups complied with the tasks. Plots of the force measured while a stroke subject performed left handed (affected side) gripping with forearm restraint, and the angle of ankle rotation during left foot flexion with pelvic restraint are shown in Fig. 2.4. Although all subjects were able to perform the tasks during the correct time intervals, the phenomenon of extinction was observed in 2 out of 4 stroke subjects, which manifested as an approximately twofold reduction in force of the affected side during bilateral versus unilateral gripping.

A 2-way RANOVA of the data from the young adult group showed a statistically significant difference in the amount of head motion during different tasks ($p<0.01$), but no significant difference between being in the MR scanner versus being in the simulator ($p=0.37$) in terms of head movement.

An example of head position data for a stroke subject is plotted in Fig. 2.5, showing interesting features commonly observed. Head motion increased during foot flexion compared to rest, and was correlated with the subject's behavior. Often, a subject's head moved to a different position during dorsi flexion, and then returned to the original position after plantar flexion. This effect can also be seen through a frequency analysis of the head motion plot (Fig. 2.6). Task-correlated motion can also be seen as a shift of the mean head

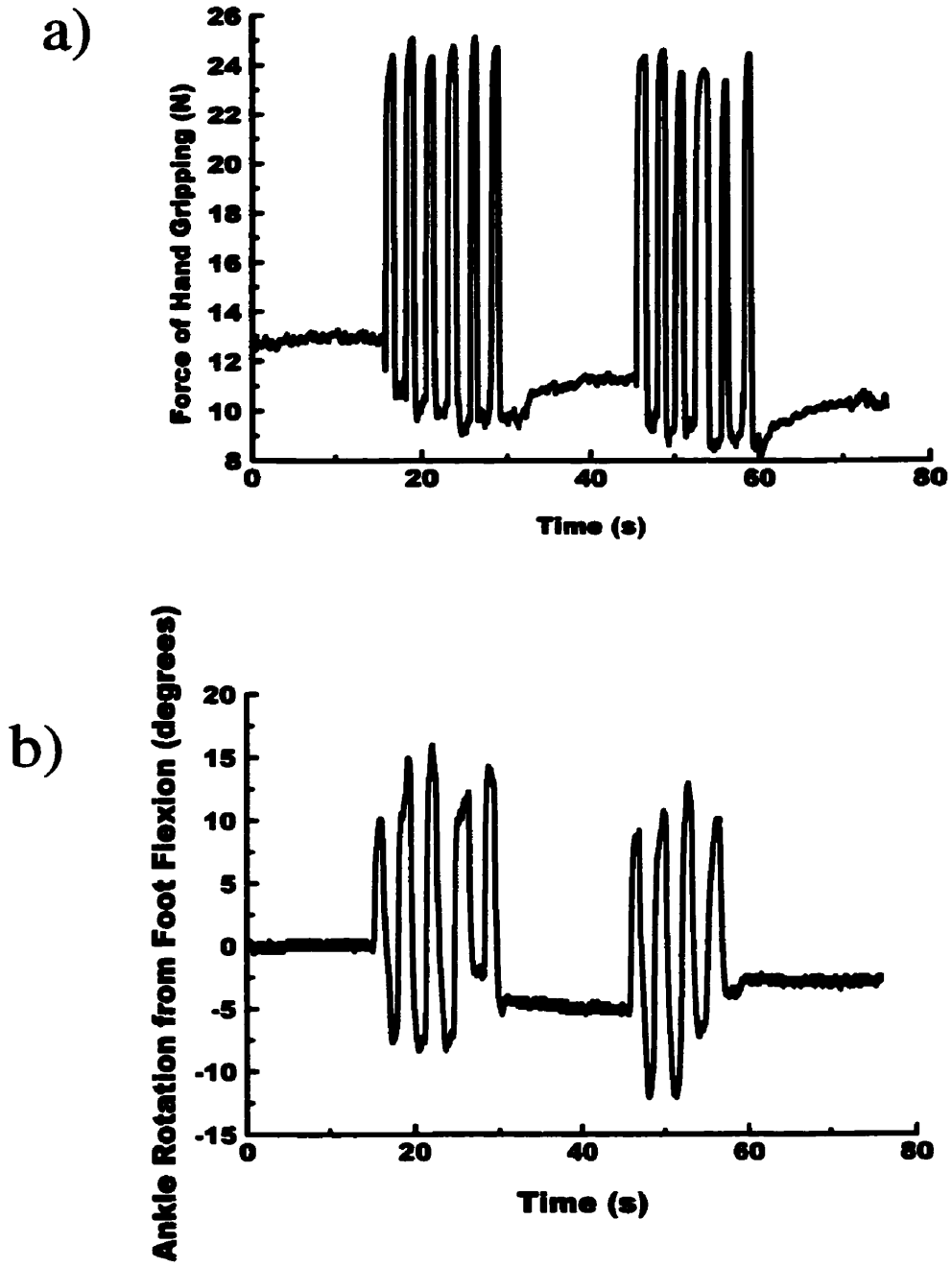

Figure 2.4. Left-handed gripping force (a), and ankle rotation during left foot flexing (b) for a representative stroke subject.

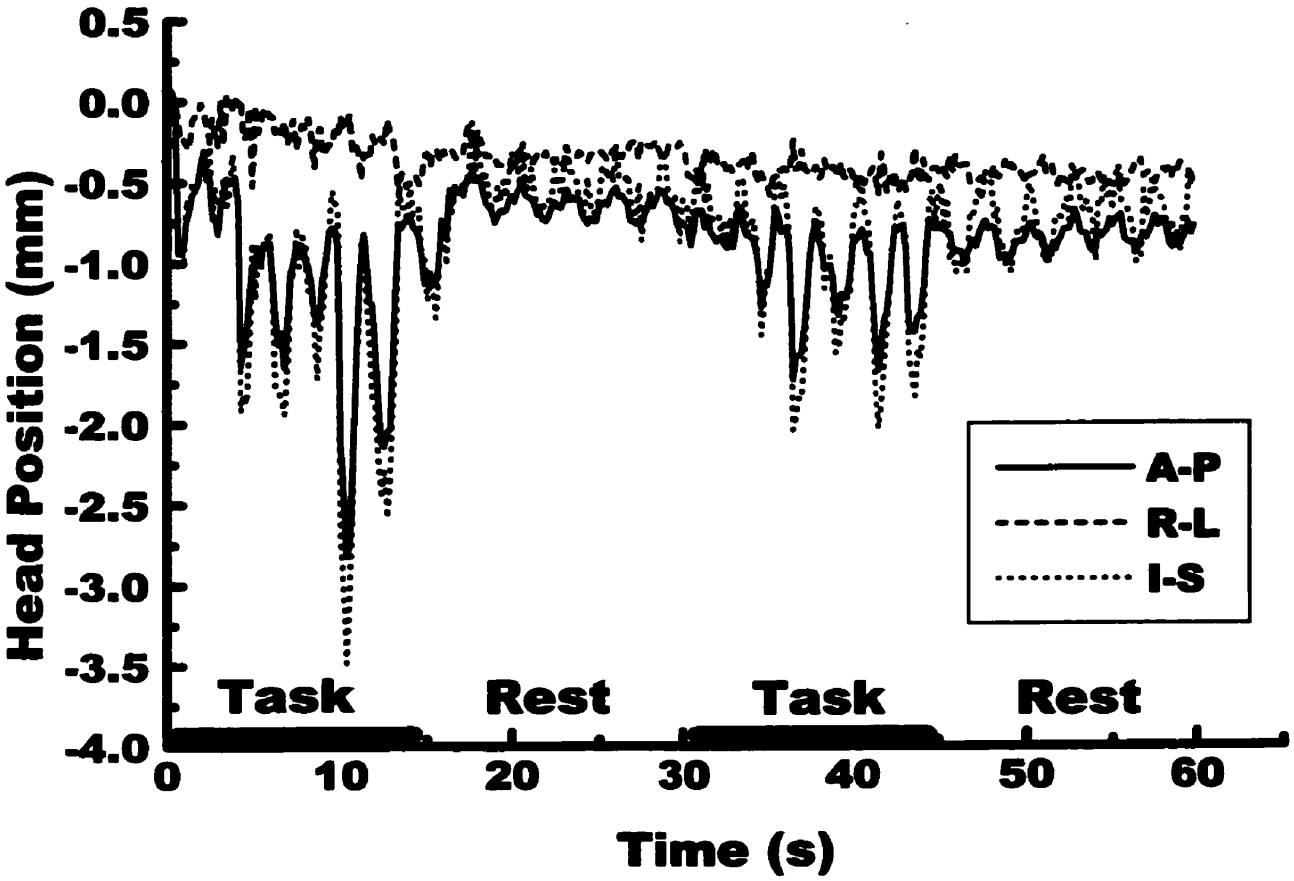

Figure 2.5. Task-correlated head motion of a stroke subject during foot flexing with foot device, exhibiting larger motion during task intervals compared to rest intervals, and a shift in the head position between the first task and first rest periods. Note also the the periodic head motion during the task periods due to foot flexion, and the cyclic motion during the rest periods due to breathing.

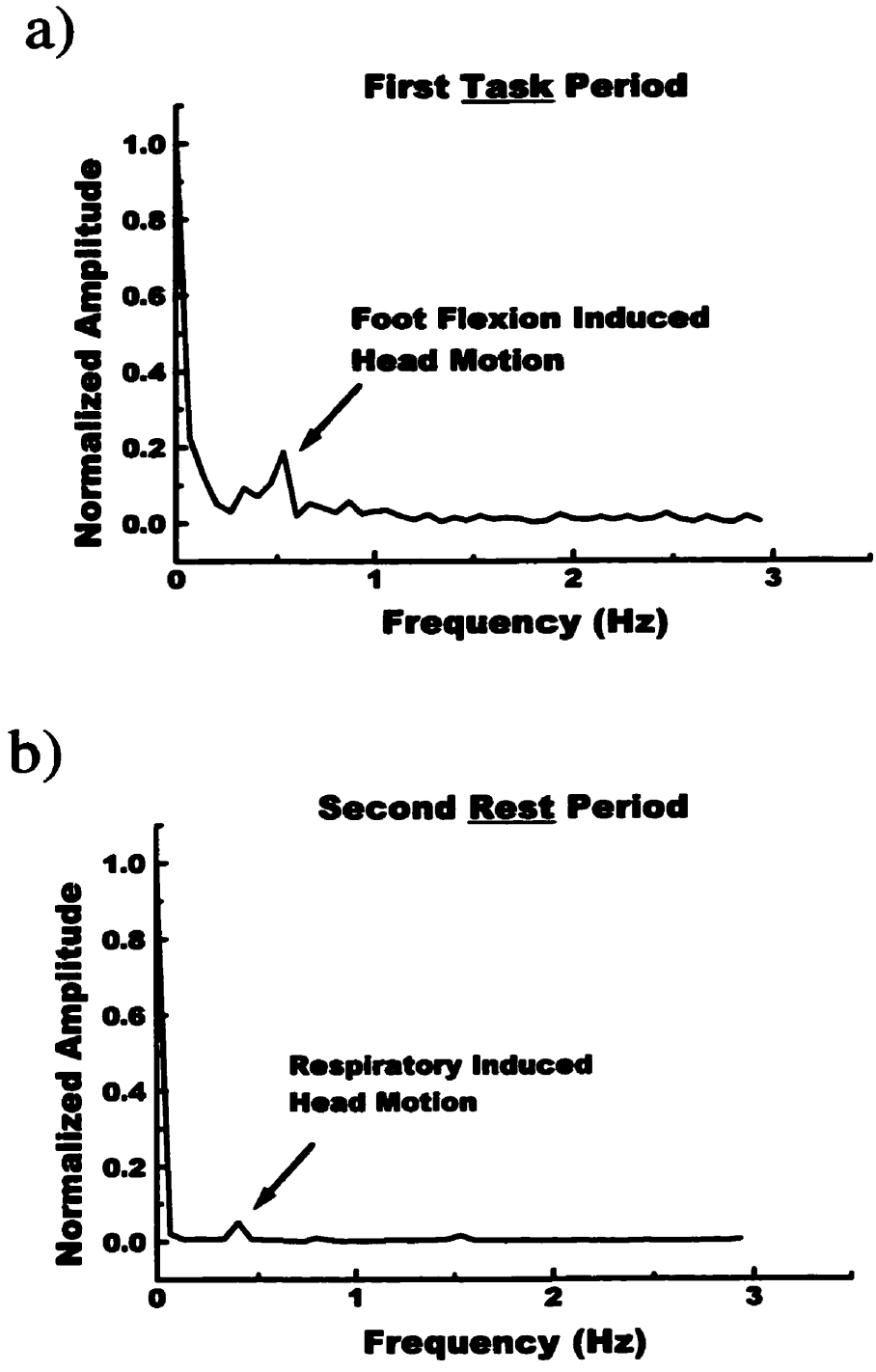

Figure 2.6. Frequency analysis of a stroke subject's head motion during foot flexing with foot device. Head motion induced by breathing and motor task is evident (a). Foot flexion frequency component is absent during rest phase (b). The large component at 0 Hz is due to positional offset.

position to a different location during the task phase, and then a return to the original position during the rest phase (Fig. 2.5). Similar head motion characteristics were observed during hand gripping tasks.

Summary bar plots of the average M_{sd} and M_r for each group of subjects are shown in Fig. 2.7 for all task conditions. There were large differences in the 95% confidence intervals between the groups, which motivated square root transformation of the data as previously mentioned. The average variance across all tasks for M_{sd} was 0.026 mm^2 for the stroke group. The age-matched and young controls had much smaller variances of 0.007 mm^2 and 0.001 mm^2, respectively. Several other trends are observable: stroke subjects exhibited more head motion than age-matched controls; the latter exhibited more head motion than young adults; and the amount of head movement due to various tasks was different (*eg* foot flexing resulted in more head motion than hand gripping for controls). The statistical significance of these trends was investigated by subsequent RANOVAs (see below).

2.3.2 Comparison of Groups, Hand vs. Foot tasks, and Efficacy of Restraints

A 2-way RANOVA of the M_{sd} data across the 3 groups and 4 task conditions (hand gripping, hand gripping with forearm restraint, foot flexing, and foot flexing with pelvic restraint), omitting all rest periods, found that there was a strong difference in head motion between the groups ($p<0.001$) and the task conditions ($p<0.01$), which is suggested in Fig. 2.7. The age-matched controls had much more head motion than the young adults ($p<0.01$), and the stroke subjects had increased head movement over the two other groups ($p<0.001$ for both comparisons). As determined from repeated-measures t-tests, foot flexing resulted in

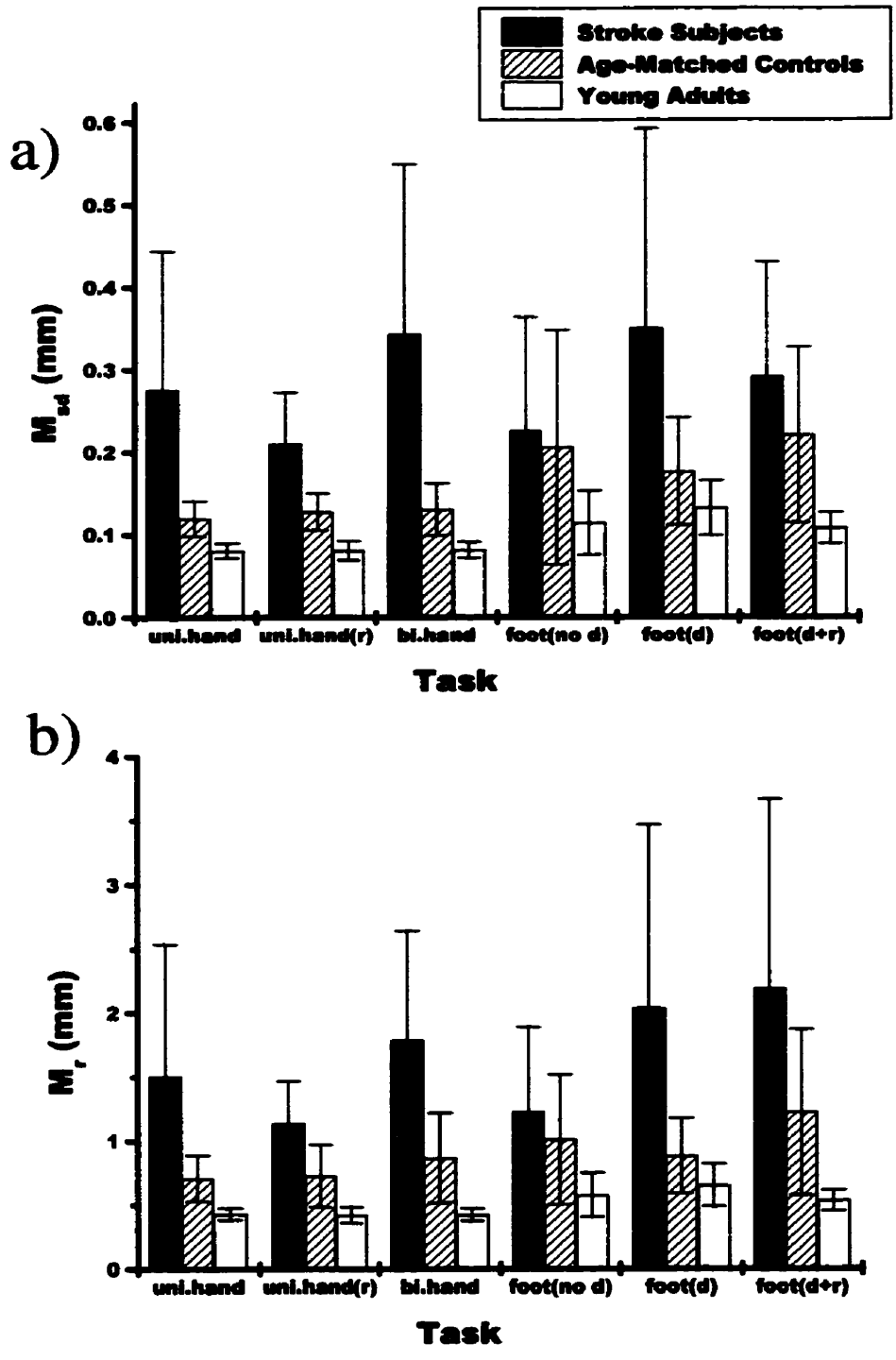

Figure 2.7. Average M_{sd} (a) and M_r (b) of head motion of stroke subjects age-matched controls and young adults during 6 different motor task conditions showing 95% confidence intervals. Note difference in vertical scales. (r)=restraint, (no d)=no device, (d)=device, (d+r)=device+restraint

significantly larger head motion than hand gripping for the age-matched and young controls ($p<0.05$ and $p<0.001$ respectively), but not for the stroke group. For all three groups, the forearm and pelvic restraints did not significantly alter the head motion.

Similar results were obtained using the M_c metric, except that the stroke subject and age-matched control groups showed similar head motion, and the use of the hand restraint notably decreased head movement ($p<0.01$). For brevity, all subsequent results are reported solely using M_{sd}.

2.3.3 Task-Correlated Motion

Comparing the task and rest periods of the head motion (M_{sd}) pooled for all subjects (for hand gripping and foot flexing tasks without restraints) revealed that 1) much more head movement occurred during the task intervals ($p<0.01$), and 2) there was a significant interaction between the task-rest differences and group ($p<0.001$). These effects can be seen in Fig. 2.8, where it is apparent that there is a larger difference between task and rest interval head motion for stroke subjects than the controls, and is also suggested in the representative data of Fig. 2.5.

There was a difference between task-correlated motion associated with the hand and foot tasks for the pooled data from all subjects ($p<0.05$). The hand data showed no significant difference between the task and rest intervals, but the foot data showed an increase in head motion during the task period ($p<0.001$).

A comparison of the mean head position for task versus rest intervals, after subtracting linear head motion trends, showed that this type of task-correlated motion was not common enough to be statistically significant for either the hand or foot tasks.

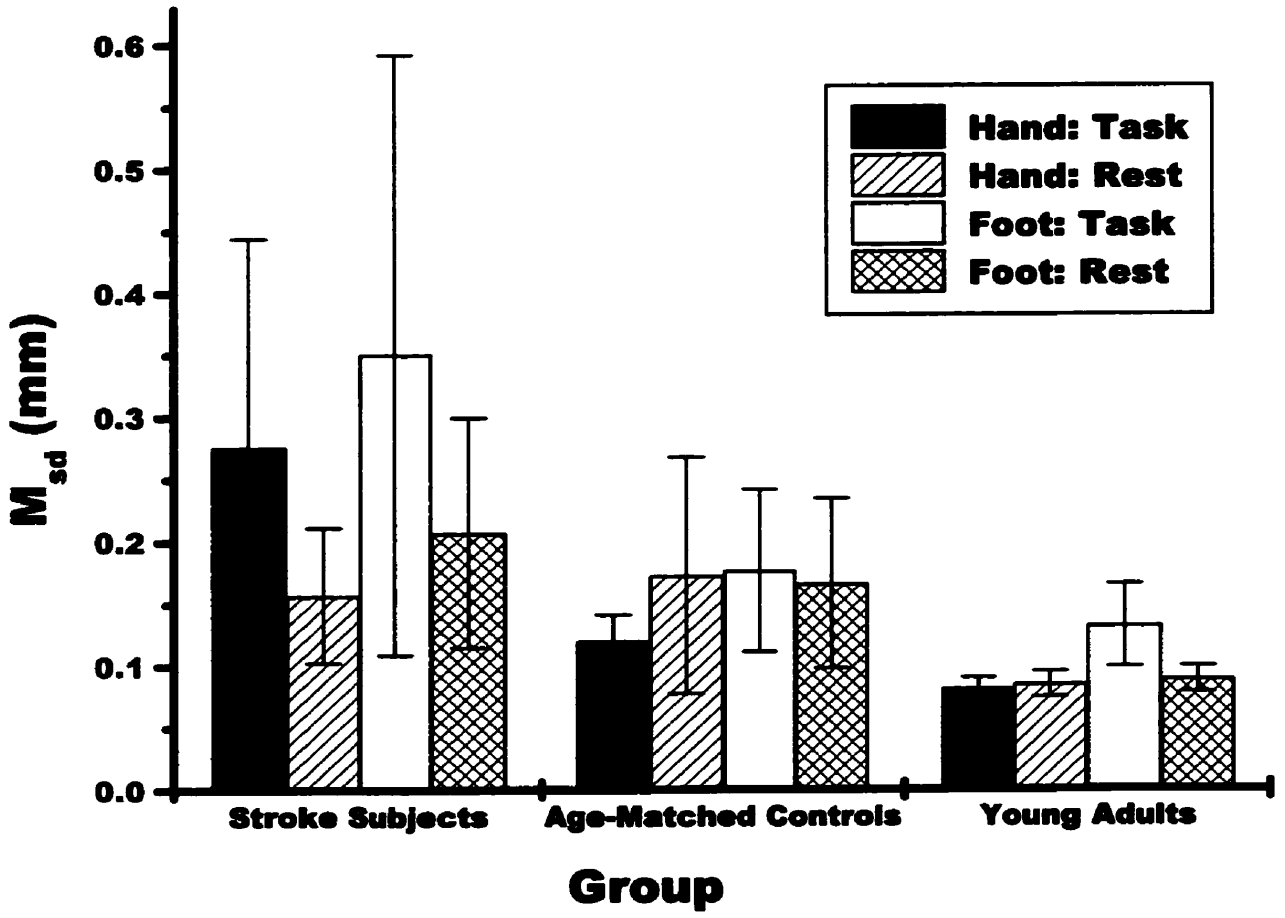

Figure 2.8. Task and rest phase average M_{sd} for unilateral hand gripping without restraint and foot flexing with device but no restraint for stroke subjects, age-matched controls and young adults (95% confidence intervals shown).

2.3.4 Directional Dominance of Head Motion

The translational head motion data from the hand gripping task without restraint generally did not reveal any preferential direction of head movement, but a significant interaction between the direction of the head motion and the group was observed ($p<0.01$, Fig. 2.9a). There was, however, a difference in direction of head translation for the foot flexing task ($p<0.01$), as well as an interaction between the direction of head motion and the group ($p<0.05$, Fig. 2.9b). Head motion in the anterior-posterior (A-P) and right-left (R-L) directions was larger than that in the superior-inferior (S-I) direction ($p<0.05$ and $p<0.01$, respectively).

An analysis of the rotational head motion revealed differences for the hand task ($p<0.001$) and the foot task ($p<0.01$), and strong interactions between the directions and groups ($p<0.001$, $p<0.01$ for hand and foot tasks respectively, Fig. 2.9c and d). Pitch and roll rotations were significantly larger than the yaw direction ($p<0.05$). See Fig. 2.3 for co-ordinate system. The pitch movement was larger than the roll ($p<0.001$) for the hand task, but was not different for the foot task.

2.3.5 Comparison of Unilateral vs. Bilateral Hand Tasks

Unilateral hand gripping compared to bilateral gripping resulted in a strong difference in M_{sd} when the data from all the subjects were pooled ($p<0.001$). There was also a substantial interaction effect between the unilateral vs. bilateral gripping and the group ($p<0.01$). Specifically, gripping with one hand or two hands did not result in a difference for the young or age-matched controls, but bilateral hand gripping caused an increase in head

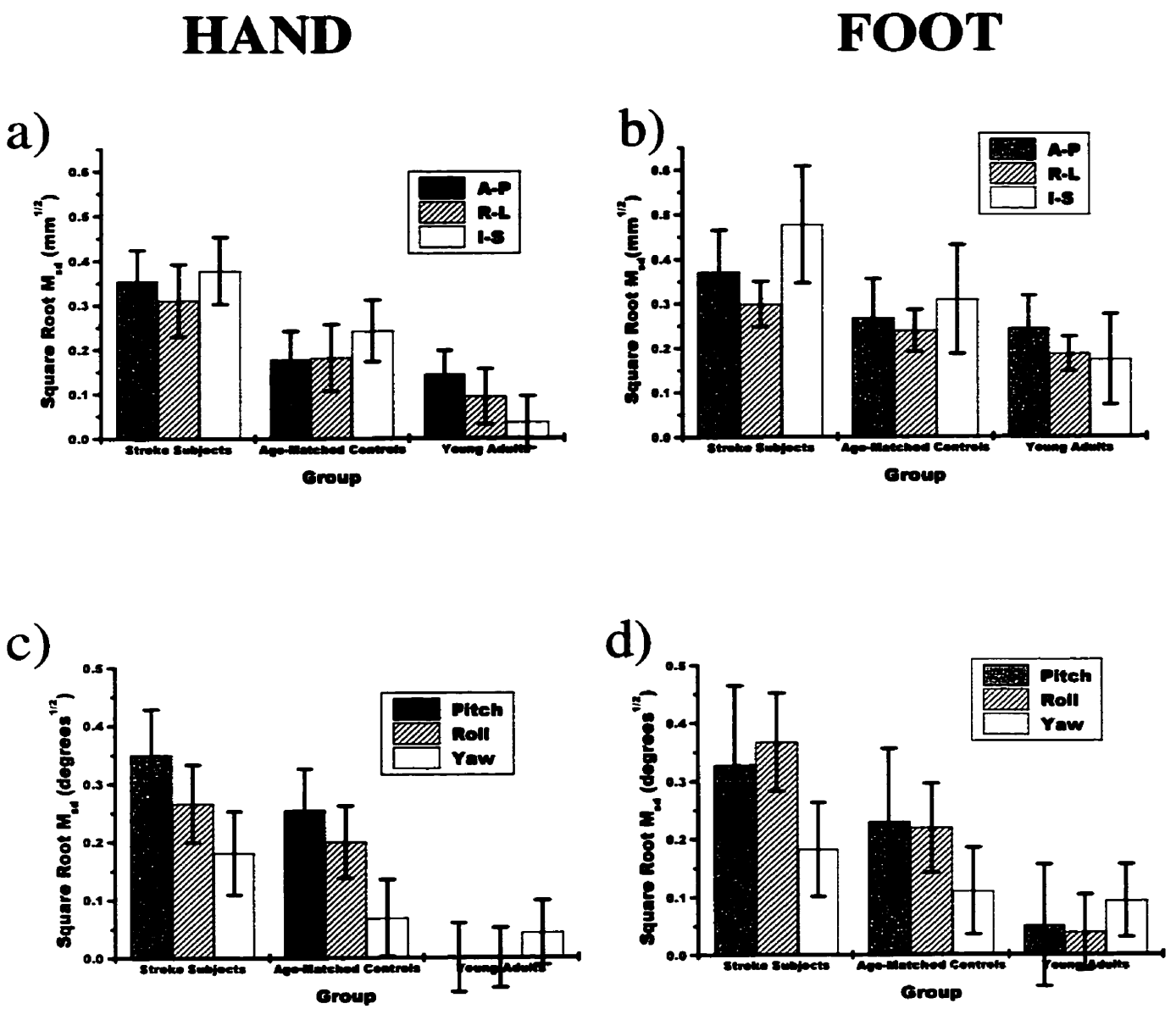

Figure 2.9. Group versus direction of head translation for unilateral hand gripping without restraint (a) and foot flexing without restraint (b). Analogous plots for head rotation are shown in (c) and (d) respectively. (Values plotted are mean fitted parameters calculated through SPSS.)

motion for the stroke subjects ($p<0.05$) (Fig. 2.7). Analyses with M_c and M_r supported these findings.

2.3.6 Comparison of Foot Tasks with vs. without Foot Device

The use of the foot device did not reduce head motion for any of the groups. Effective unilateral foot flexing, however, was often not achieved by the stroke subjects without the apparatus.

2.4 Discussion

2.4.1 Differences of Head Motion Characteristics between Subject Groups

The age-matched controls (average age 59 years old) exhibited a large increase in the amount and range of head motion compared to the young subjects (average age 28) ($p<0.001$), as can be observed in Fig. 2.7. These findings are similar to those of D'Esposito et al. who found through retrospective methods that the median head motion of elderly subjects (61-82 years old) was 1.8 times larger than the median motion of the young group (18-32 years old) [67].

Severe motion fMRI artifacts would be expected from the stroke group, but not for the age-matched and young controls. From Fig. 2.7b, the amount of head motion for the control groups was usually well below 1 mm, while the average M_r for the stroke subjects was 1.5 ± 1.0 mm and 2.0 ± 1.4 mm for the hand and foot tasks without restraints, respectively. When the amplitude of the head motion becomes comparable to the size of the voxel, unrecoverable image corruption occurs. The usual range of head movement for an fMRI scan

resulting in reliable data is about 0.5 mm. As head movement increases above 1 mm, the severity of artifacts from head motion also increases, when the in-plane voxel (3-D pixel) dimensions are about 3x3 mm (*eg* 64x64 matrix at 20 cm field of view (FOV)). It is therefore, not surprising that fMRI data from stroke subjects are often plagued by motion artifacts. It is clear that improvements in head motion correction techniques are needed for such patient populations. A recent study by Field et al. found that submillimeter in-plane motion and only weakly to moderately task-correlated motion (correlation coefficient > 0.52) could cause false fMRI activation. The scanning parameters used for their phantom study were a 64x64 matrix at 24 cm FOV [76].

Through the RANOVA analysis, the head motion of the stroke subjects was found to be more task-correlated than that of the age-matched controls (Fig. 2.8). These results are analogous to motion characterization data reported for schizophrenics performing a silent verbal fluency task [28]. Schizophrenics produced more stimulus-correlated motion than control subjects, who produced motion dominated by linear trends. In the work reported here, young adults and age-matched controls usually exhibited head motion dominated by linear trends (slow drift). Head motion arising from respiration was also observed, however, (see Fig. 2.5: during rest phase) and was often a predominating component of the motion in healthy adults. Respiratory-induced motion is often difficult to observe using coregistration methods, particularly if fMRI is performed with insufficient temporal resolution. This is one possible reason for the failure previously to see this motion in schizophrenics [28].

Other group-related findings include the large variation of head motion between the individual stroke subjects. This was anticipated because stroke patients typically present with motor deficits with a wide range of severity. Stroke patients with "intermediate" Chedoke-

McMastor scores (2-5) for the foot and hand were deemed suitable for this study. Patients who could not comply well with simple motor tasks (low score) and who had near normal motor function would not benefit significantly from an fMRI motor examination. A slightly different selection criterion would likely affect the details, but not the trends, of the results obtained.

Clearly, the differences in head motion between subject populations indicate the necessity for careful selection of fMRI subjects, and cautious interpretation of fMRI activation. The latter is especially true when comparing the activation between patients who could be suspected of having differing motion characteristics from the control group [28]. What appears as differences in brain activation could only be a motion-induced artifact.

A potential criticism of the reported results is that the tasks were not randomized, such that the effect of habituation to the simulator cannot be addressed. The order of the tasks was chosen to minimize the amount of set-up time. As described above, each of the data collection runs consisted of two cycles of a 15 second task period, and a 15 second rest period. A decrease in head motion between the first and second cycle of the data collection runs would be evident if habituation occurred. This effect was not seen. In most cases, it would also be more difficult to detect differences if habituation did occur because the second task was found to result in more head motion (*eg* all foot tasks were performed after the hand tasks). It can therefore be concluded that the data were probably not biased by the ordering of the task conditions.

2.4.2 Translational and Rotational Motion

Both new results and those that support previous studies were obtained that highlight differences in translational and rotational head motion during fMRI tasks. For example, translational head motion was produced in a preferred direction for foot tasks but was not for the hand tasks (Fig. 2.9a and b). This could be because the translational head motion produced by hand tasks was too small for preferential directions to be determined within experimental error. For the foot tasks, motion in the A-P and S-I directions was larger than that in the R-L direction. Although the vacuum pillow used in this work preferentially restricted R-L motion compared to S-I and A-P motion, there is support that the results reported here are not solely a consequence of using this type of restraint. A previous analysis during frameless stereotactic radiosurgery [66] also used an optical tracking system (Optotrak, Northern Digital, Inc.) to assess the head motion of young adults for 30 minutes while they remained at rest. The largest motion was produced in the S-I direction (1.44 mm maximum amplitude, attributed to swallowing), and suggests that S-I motion predominates regardless of the influence of the vacuum pillow.

The hand gripping task produced rotational head motion that was predominated by nodding (Fig. 2.9c and d). This is again consistent with the restraining characteristics of the vacuum pillow, but is also in accordance with a previous PET study using a laser-based system to measure head motion for subjects wearing thermoplastic molds [36]. Rotations up to 4.1 and 2.4 degrees in the pitch and roll directions occurred in 130 minutes, respectively, again suggesting the preferential nature of pitch rotation.

2.4.3 Head Motion Differences due to Tasks and Restraints

Most fMRI motor studies use hand tasks [72] because of the large cortical representation of the hand primary sensorimotor area, and translation of motion from the hand to the head is minimal. Our data indicates that although foot tasks produce larger head motion in the young adult and age-matched control groups, this motion is within acceptable limits. Functional MRI of the lower limb appears feasible for selected stroke subjects that exhibit acceptable head motion, although only 4 of 6 stroke subjects studied in this work had adequately small head movement to provide useful fMRI data.

Of the restraints investigated, none significantly reduced the head motion associated with the three groups. The foot device had additional merit, however, because with the device, well-controlled unilateral foot flexion was much more achievable for many of the stroke subjects. This could have been due to the additional somatosensory and proprioceptive input provided by the flexion device versus the unaided condition (which tended to produce smaller extent of flexion or severe mirror motion of the contralateral leg). In the case of the pelvic and forearm restraints, their ineffectiveness could be due to the inability to reduce the predominant translational motion of the head (S-I direction).

2.4.4 Simulator

The MR scanner simulator is a powerful tool for familiarizing, training and screening future fMRI subjects, as well as developing and testing behavioral tasks designed for fMRI. The advantages of simulators were discussed in Chapter 1. The use of simulators has previously been advocated as an alternative to sedating children during MR scans [73]. Commercial MRI simulators are now available that feature internal lights, cooling systems,

motorized tables, speakers and amplifiers, and are substantially less costly than MR scanners (thousands of dollars versus millions of dollars)[77].

The disadvantages of using an MR simulator include the extra time necessary before an MR scanning session. Subjects could become tired from the simulation session, and perhaps not have adequate time to rest before the MR session. Practically, no matter how closely a simulator resembles a MR scanner, it is not the real thing and likely does not provoke the same level of anxiety in the subject, potentially resulting in more movement than expected after training sessions in the simulator. It is worth noting, however, that this effect was not observed for the measurements of young adults in the scanner and the simulator.

Coupling a position tracking system with a simulator that includes additional equipment to deliver sensory stimuli and to monitor behavioural responses would enable the measurement of head motion introduced by a variety of cognitive tasks. The practical benefits of simulators could then be carefully quantified.

2.5 Conclusion

Subject populations (*eg* young vs. elderly vs. stroke patients) could have very different head motion characteristics, some of which could be extremely detrimental to fMRI. Motion-induced artifacts would not be expected for the age-matched and young adult groups because they exhibited adequately small head motion. The head movement of the stroke group, however, was approximately twice that of the age-matched group, and was dominated in the S-I and pitch directions. Head motion characteristics provide the information necessary to assist in designing optimal ergonomic restraints and additional motion

compensation strategies, as well as practical motor tasks targeted to the elderly and patient populations. Position tracking systems, used with fMRI simulators and actual scanners, provide an important initial means of testing such new designs in the future.

Chapter 3

Conclusions and Future Directions

3.1 Summary

By addressing the three experimental objectives of this thesis, the work presented in Chapter 2 supports the hypothesis that characterizing head motion is important for designing methods to improve the quality of fMRI data.

The first objective of the thesis was to characterize head motion during motor tasks typically used in fMRI. This was achieved by assembling apparatus to create an fMRI simulator coupled with an infrared tracking system, and then measuring head motion in various subject populations. Several metrics and analyses were devised to quantify head motion as a function of time. Young healthy subjects exhibited cyclical head motion due to respiration, while frequent large transient and task-correlated movements occurred with the stroke patients. Translational and rotational head motions were predominant in the superior-inferior and nodding directions, respectively.

The second objective was to investigate whether different subject groups, restraints, and motor tasks produced different head motion characteristics. Head motion was found to worsen progressively across groups of young healthy adults, healthy seniors, and recovering stroke subjects. Use of forearm and pelvic restraints did not reduce head movement. A foot flexing task produced slightly more head motion in young adults and healthy seniors than was produced by hand tasks, although the movement associated with the former task was found to be adequately small for fMRI.

Head motion was sufficiently large in the stroke subject group that no differences produced by hand tasks versus foot tasks were observed.

The third objective was to investigate the potential of MR simulators for improving fMRI methodology. The wealth of data provided by using a simulator to address objectives 1 and 2 clearly suggested the usefulness of such devices. The data also highlighted several options for designing methods to reduce the problem of head motion.

The remainder of this chapter briefly describes several possible future directions of motion suppression research that I believe have good potential for success.

Future Directions

3.2.1 fMRI Simulators for Training and Screening

While addressing the experimental objectives of the thesis, an important additional benefit of simulators was observed anecdotally: the potential for training and screening future fMRI subjects. If conclusive evidence of the benefits of simulators was gained through a quantitative study, then there would exist strong motivation for the wider fMRI research community to use such devices.

A representative example of head motion reduction from training in the simulator is shown in Fig. 3.1, which illustrates plots of head rotation versus time for a stroke subject performing bilateral hand gripping. The data were obtained retrospectively using a coregistration algorithm employed in commonly used fMRI analysis software, Analysis

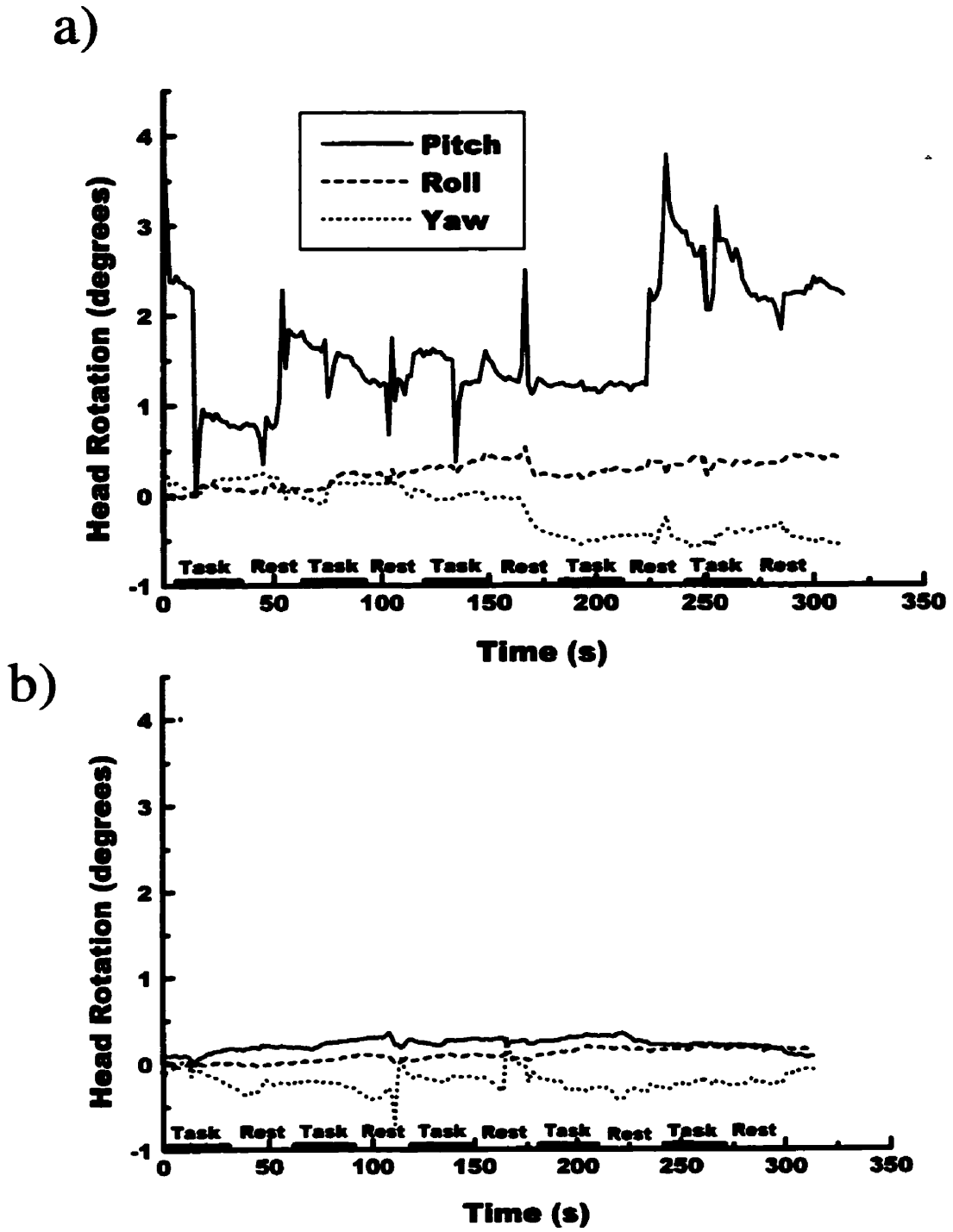

Figure 3.1. Rotational head motion during fMRI of a stroke subject performing bilateral hand gripping task (data obtained retrospectively by image coregistration algorithm in AFNI [78, 79]). Head rotation very large prior to MR simulation session (a), but was greatly reduced post training session (b).

of Functional Neuroimages (AFNI) [78, 79]. Figure 3.1a shows the plots obtained when the subject did not have a training session before fMRI: the image data were unusable because of excessive head motion (range: approximately 4° pitch). Figure 3.1b shows the analogous plots after training the same subject in the simulator and performing fMRI the following day (range: <1° pitch). In the latter case, the data are acceptable.

In another case, a stroke patient in the acute phase of recovery (several days post-stroke) was trained on hand gripping and finger-tapping tasks in the MR simulator. The subject was instructed to lie as still as possible without speaking during the practice runs as positional data were acquired. Head motion is plotted in Fig. 3.2a for unilateral gripping, and clearly indicates unacceptable movement. The second task interval exhibits head motion ranging from 3-6 mm associated with 3 hand grips, the second rest interval contains a large head movement (> 8 mm), and the subject also started speaking during the last rest interval. As a consequence, the subject was given additional instructions: to concentrate on remaining still; to keep his arm from moving during hand gripping; and to squeeze the hand grips much less tightly to eliminate movement of the entire body associated with the effort of the gripping action. As can be seen from Fig. 3.2b, subsequent head motion was mostly much smaller (<0.5 mm) compared to the previous run. There was, however, a large head movement during the first rest interval from the subject speaking even though he was instructed to remain silent several times. The reduction in head motion during the second run exemplifies the usefulness of a training session as one of a combination of strategies to improve the quality of fMRI data.

These observations indicate the importance of performing a study to compare the head motion produced in initial simulated fMRI runs with that produced after additional

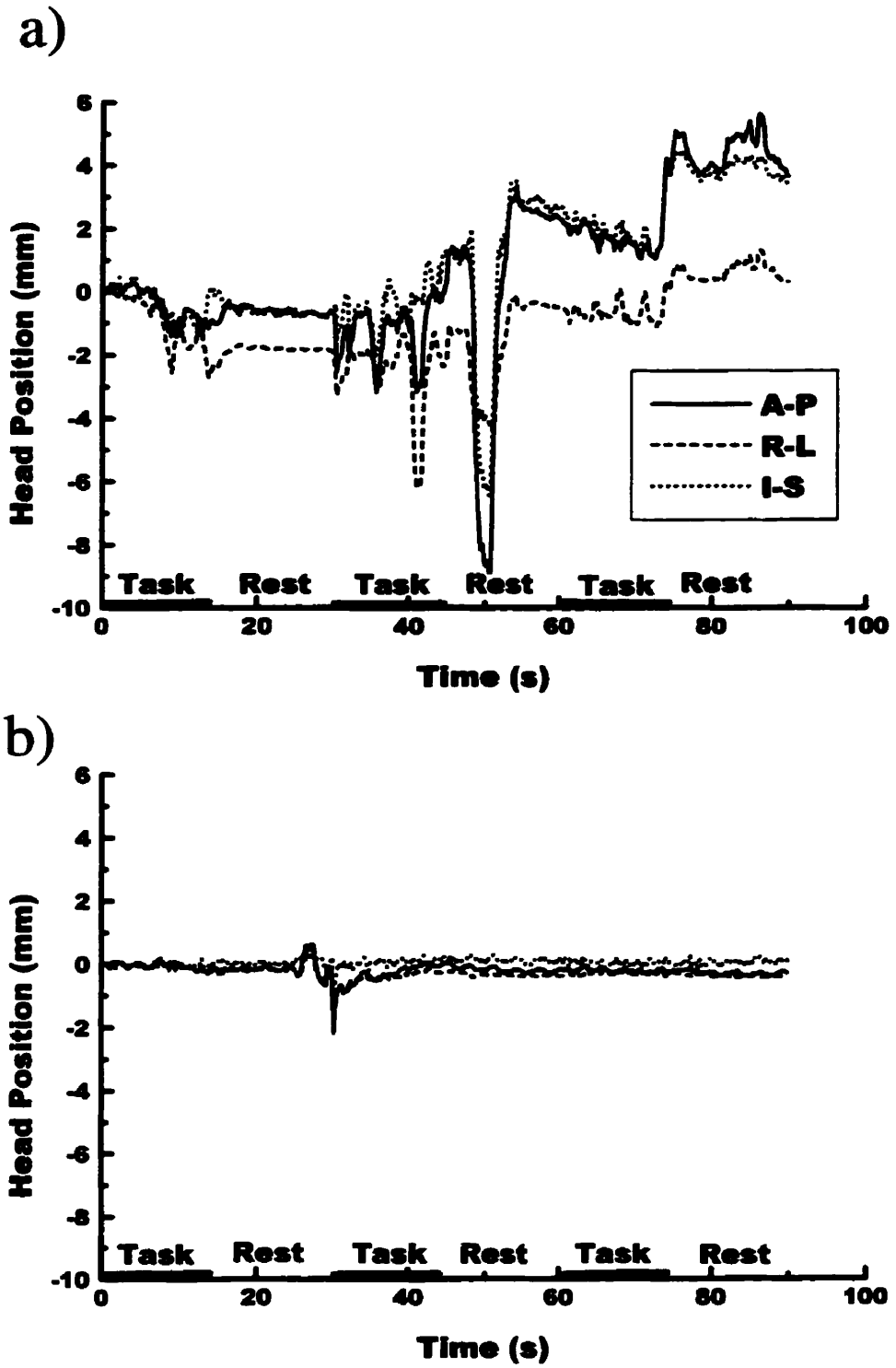

Figure 3.2. Head motion of stroke subject in MR simulator performing hand gripping task during training session. Much less head motion occurred during the second run after more instruction and practice (b), compared to the first run (a).

instruction and feedback to determine whether training reduces head movement. Based on the work presented in this thesis, a reasonable hypothesis is that stroke patients benefit more from simulator training than age-matched controls and young healthy adults.

3.2.2 Optimizing Restraints

Information gathered on head motion characteristics will aid in the design of optimized head restraints. For example, the predominant rotational motion observed was nodding. Research on a restraint to restrict the motion mainly in this orientation is now underway. The prototype consists of a modified plastic head cradle (Silverman's Supports, Med-Tec Inc., San Jose, California) commonly used for positioning the head during radiation therapy, mounted on a lucite board that replaces the head coil's head rest. An adjustable velcro strap is applied across the forehead to minimize nodding (Fig. 3.3). Preliminary measurements using the simulator and Polaris system indicate that the head restraint stabilizes the subject's head as well as a vacuum pillow. Functional MRI of a young adult performing a finger tapping experiment indicates that the prototype is comfortable and MR compatible. Head motion data for this experiment, obtained using image coregistration, are plotted in Fig. 3.4 and are well within acceptable limits. Future study is required, perhaps using the simulator and Polaris tracking system, to determine whether the prototype is adequate for the elderly and patient populations, and whether additional restraining belts are required.

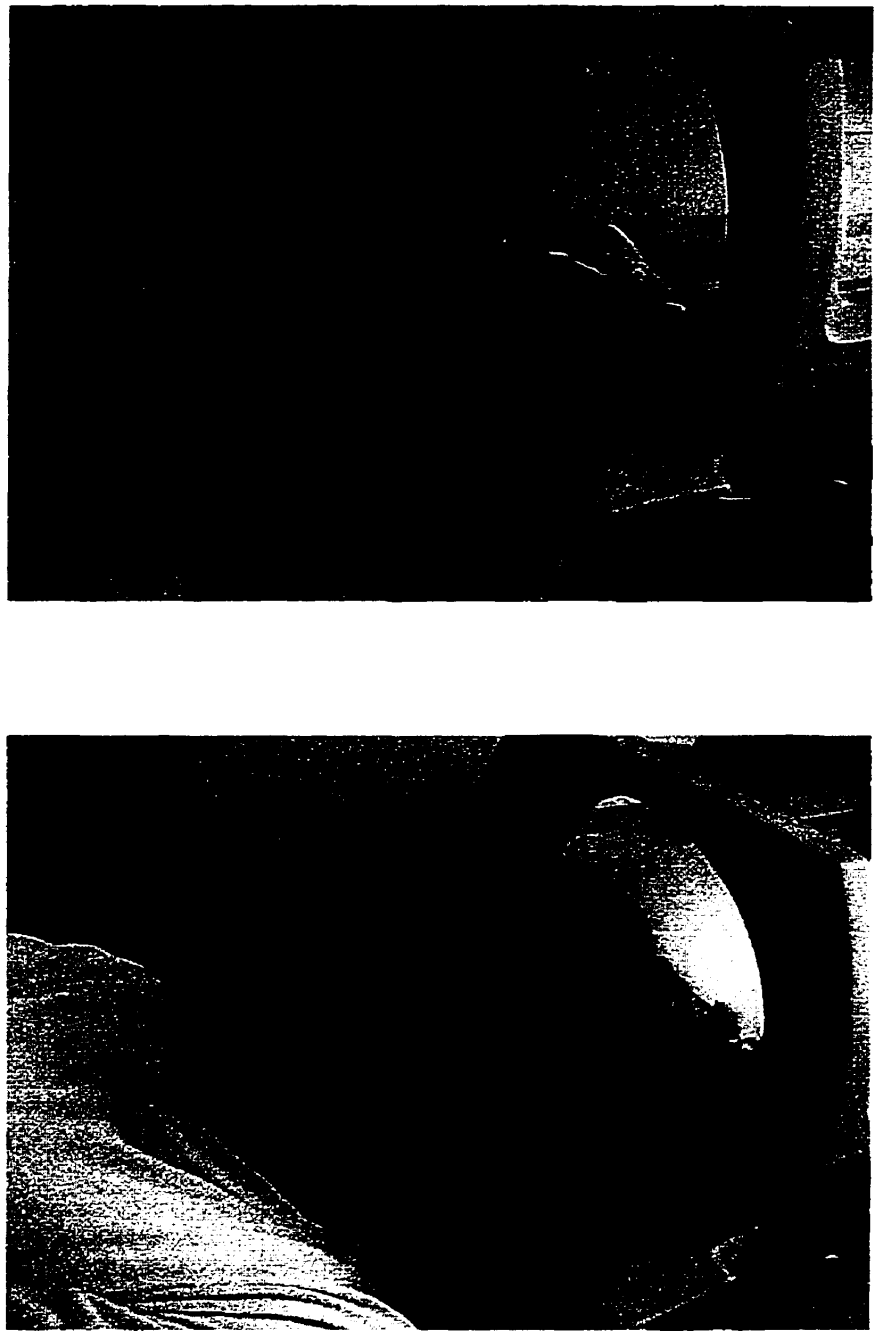

Figure 3.3. New fMRI head restraint consisting of commercial head cradle (Med-Tek Inc.) and forehead strap mounted inside head coil.

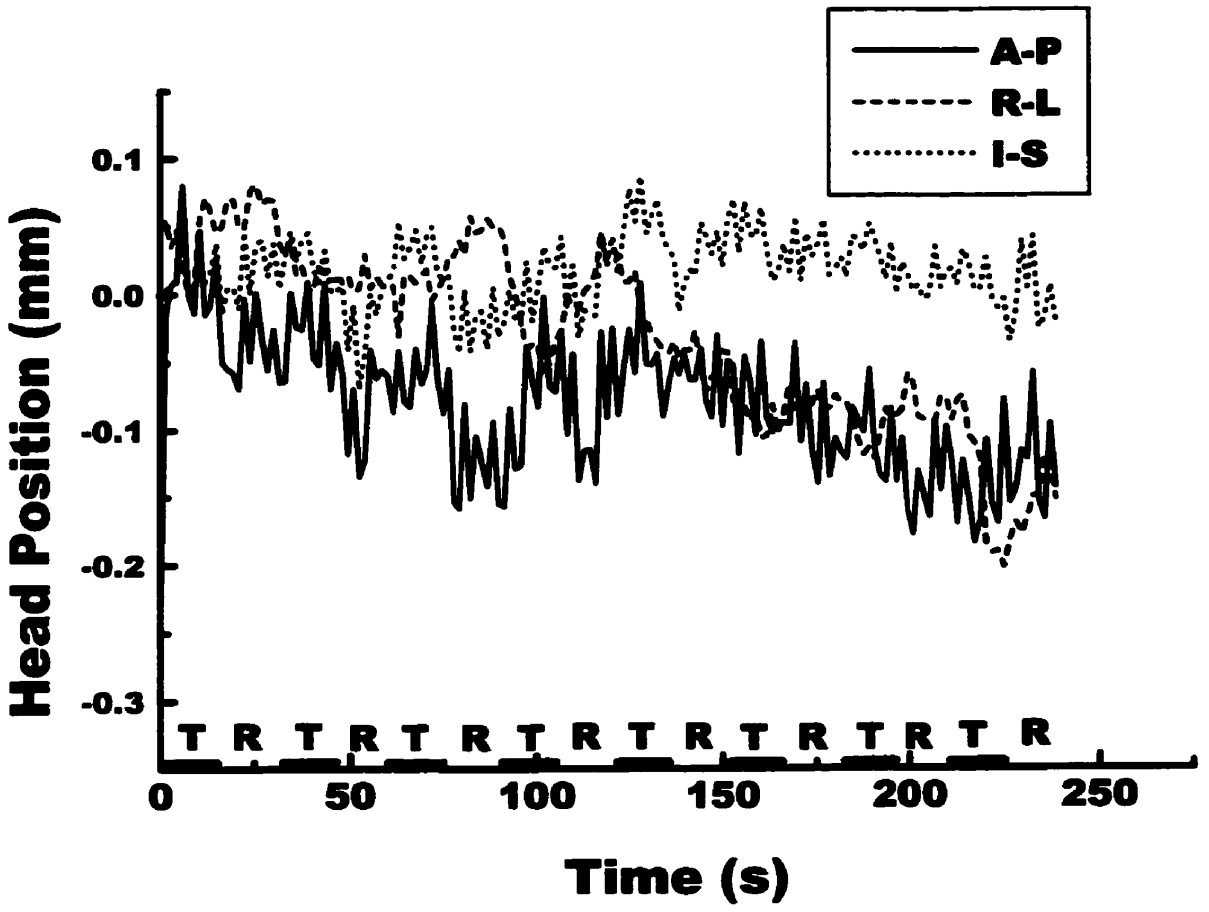

Figure 3.4. Head position during fMRI of a young healthy adult performing finger-tapping, displaying relatively small head motion using new fMRI head restraint (values determined with retrospective coregistration in AFNI). T=task, R=rest

3.2.3 Motion Tracking during fMRI

In Chapter 2, the active Polaris tracking system was configured to operate in an MR scanner operating at 1.5 T. The active Polaris tool, however, caused severe artifacts in fMRI images because of the ferromagnetic leads to the infrared-emitting diodes. Fortunately, a passive version of the Polaris system is available that emits infrared light from diodes surrounding the Polaris cameras, which then detect the reflections from a minimum of three spherical plastic markers to obtain positional information. These markers are MR compatible and introduce no image artifacts with fast MRI (Fig. 3.5). The passive Polaris system enables retrospective motion correction of fMRI data, and facilitates development of prospective scan plane tracking methods.

An initial step is to compare the effectiveness of Polaris tracking data and coregistration algorithms for head motion correction. It is likely that the Polaris system will compensate for head motion better because the positional data are not corrupted by motion-induced image artifacts. Secondly, although retrospective realignment methods can reduce head motion artifacts, they do not completely solve the problem because magnetic susceptibility effects are often still present [80]. Figure 3.6a shows false activation in an fMRI of a stroke patient using left-handed sensory stimulation via rubbing the palm with a toothbrush. After retrospective coregistration (Fig. 3.6b), false activation remains, especially above the sinus cavity, even though the head motion determined by the coregistration algorithm was relatively small (<0.4 mm in all 3 translational directions). The Polaris system, however, can reduce some of the magnetic susceptibility effects because a signal intensity correction factor can be determined for each image based on the independently measured motion data.

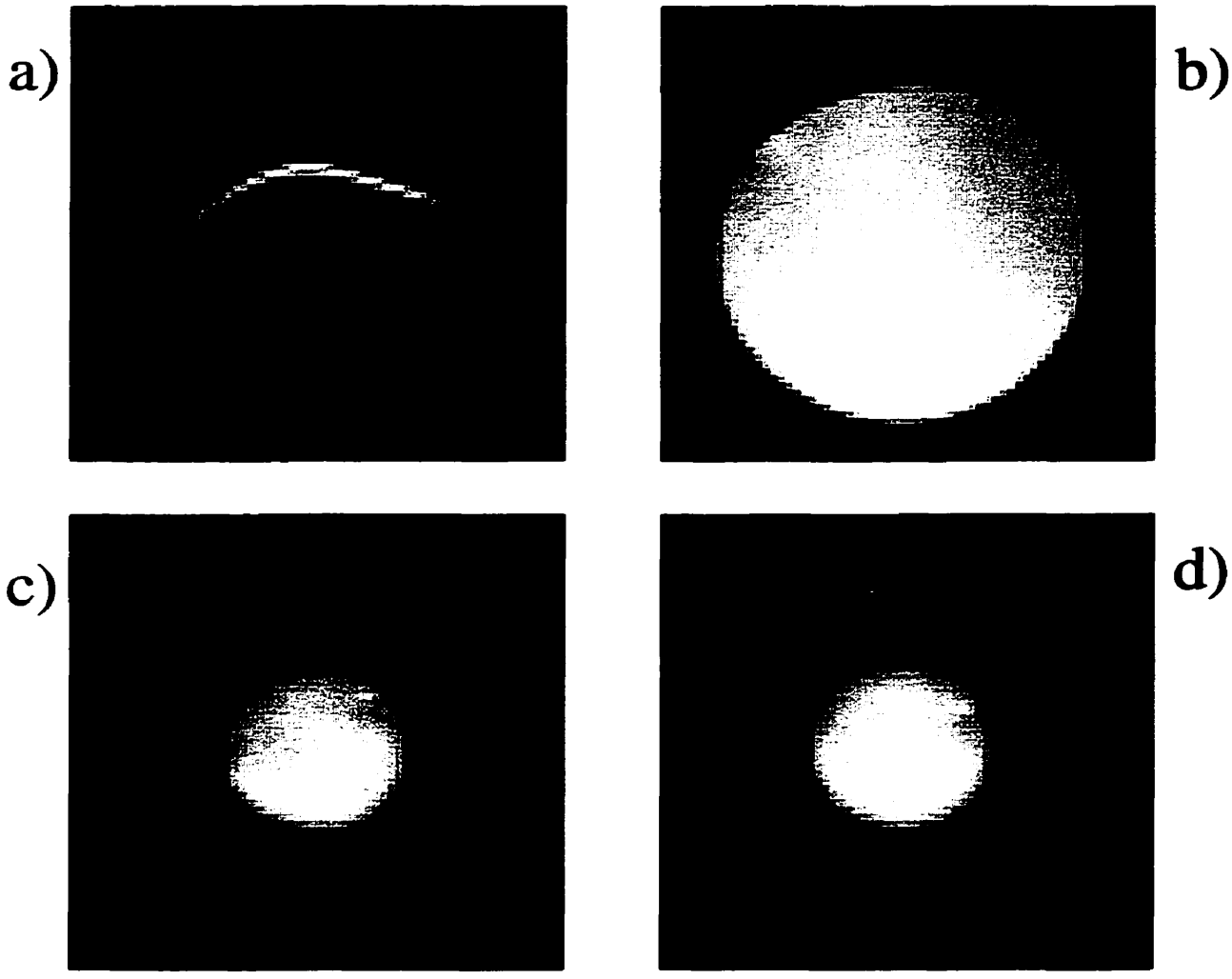

Figure 3.5. Ferromagnetic leads in active Polaris tool attached to spherical object causes MR image corruption (a). Uncorrupted image when active Polaris tool is out of MR scanner bore (b). Comparison of MR images with passive Polaris markers attached to sphere (c) and passive markers out of scanner bore (d) shows no differences. Slice position used in a) and b) was closer to the center of the sphere than c) and d). [Imaging parameters similar to EPI of Fig. 1.3c, except 7mm slice thickness used.]

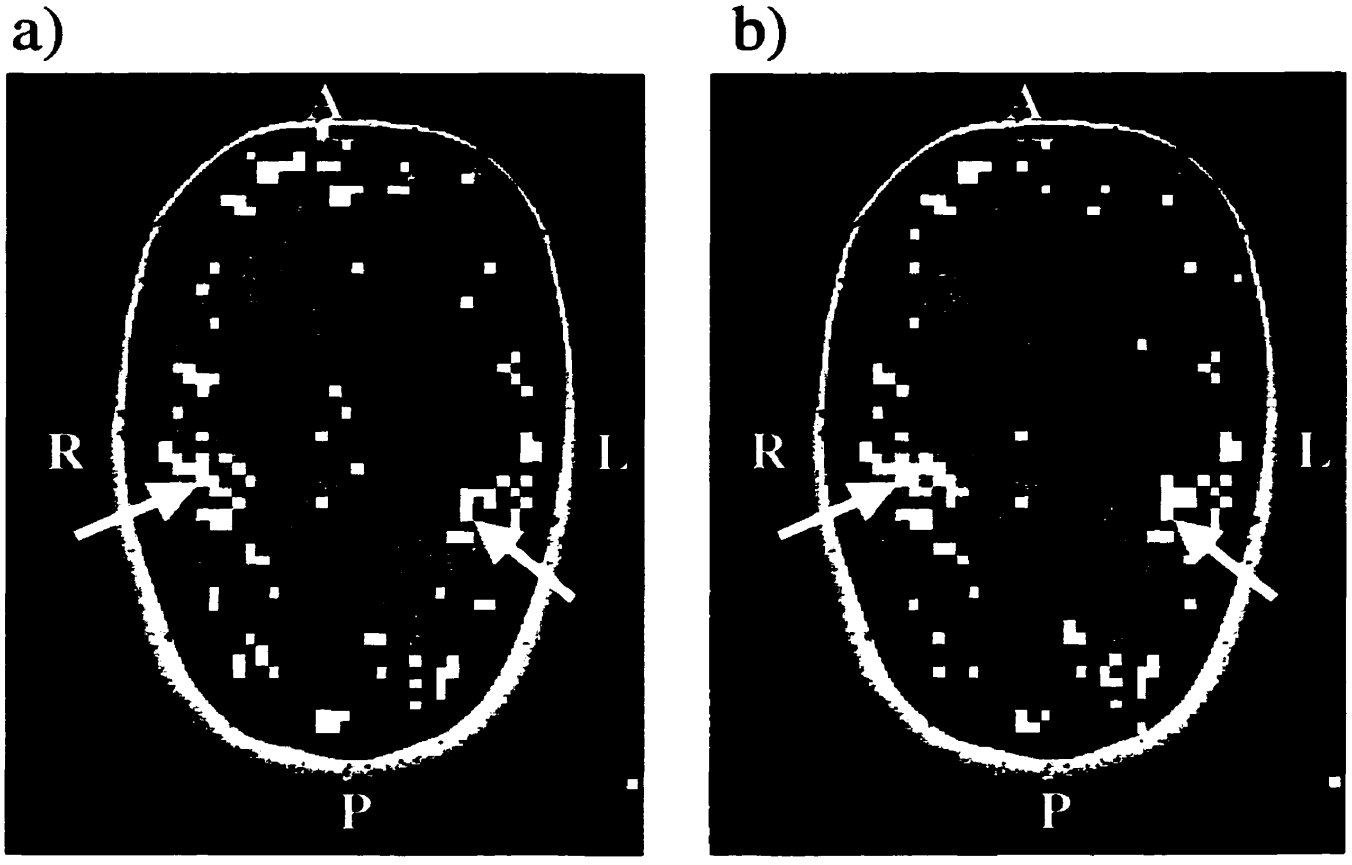

Figure 3.6. Functional image of a stroke subject to assess somatosensory (tactile) activation. Subject stimulated via rubbing the left palm with a toothbrush (blocked design: 30 s rubbing/30 s rest; 5 repeats). Activations should be present in regions indicated by arrows, although much spurious activation is observed when analysis is performed without retrospective coregistration (a). Little improvement is observed even when retrospective coregistration is adopted, despite the fact that the subject moved little (b). See Fig. 1.5 for the imaging parameters.

The Polaris system will likely be used more extensively for prospective than retrospective head motion correction techniques because of the advantages of real-time methods discussed in Chapter 1. The passive Polaris system has several advantages over alternative methods proposed for real-time fMRI scan plane tracking. Head position monitoring methods that require manipulation of the imaging pulse sequence, such as ONAV echoes described in Chapter 1 [60, 61, 62], can lengthen image acquisition. Positional data from the passive Polaris system are totally independent from image acquisition and would therefore not prolong the imaging time. The high temporal resolution (60 Hz) of the Polaris system enables monitoring of the head motion between two consecutive "snap-shot" images (typically 1-2 seconds), which cannot be done with methods that use the fMRI images themselves to find the head motion. This could be of interest in determining and understanding the extent of motion artifacts in each image, and explaining the differences seen between images. The Polaris system is also relatively inexpensive compared to the commercially available laser tracking systems ($30 000 versus >$100 000).

Conclusion

Assessment of head motion characteristics during fMRI provides an important opportunity to improve techniques to minimize and correct for motion-induced image corruption. Several techniques are currently being used in combination to correct and suppress head motion, but it is apparent from this thesis that further research is needed to design new and improved strategies that reduce head motion problems and expand the

clinical applicability of fMRI. I am optimistic that these new strategies will soon enable fMRI of subject populations that have been previously difficult to study successfully because of motion-induced artifacts.

References

1. Cohen MS, Bookheimer SY. Localization of brain function using magnetic resonance imaging. TINS 1994;17(7):268-277.

2. Orrison WW, Lewine JD, Sanders JA, Hatshorne MF. Functional brain imaging. functional brain imaging. St. Louis: Mosley-Year Book, 239-326, 1995.

3. Kim SG, Ugurbil K. Functional magnetic resonance imaging of the human brain. Journal of Neuroscience Methods 1997;74:229-243.

4. Le Bihan D, Karni A. Applications of magnetic resonance imaging to the study of human brain function. Cognitive neuroscience 1995;5:231-237.

5. Kim SG, Richter W, Ugurbil K. Limitations of temporal resolution in functional MRI. Magn Reson Med 1997;37:631-636.

6. Dale AM. Optimal experimental design for event-related fMRI. Human Brain Mapping 1999;8:109-114.

7. Stapleton SR, Kiriakopoulos E, Mikulis D, Drake JM, Hoffman HJ, Humphreys R, Hwang P, Otsubo H, Holowka S, Logan W, Rutka JT. Combined utility of functional MRI, cortical mapping, and frameless stereotaxy in the resection of lesions in eloquent areas of brain in children. Pediatr Neurosurg 1997;26:68-82.

8. Sobel DF, Gallen CC, Schwartz J, Waltz TA, Copeland B, Yamada S, Hirschkoff EC, Bloom FE. Locating the central sulcus: comparison of MR anatomic and magnetoencephalographic functional methods. AJNR 14:915-925, 1993.

9. Inoue T, Shimizu H, Nakasato N, Kumake T, Yoshimoto T, Kabasawa H. Comparative study of fMRI and MEG for objective identification of the central sulcus in patients with brain tumors. Proceedings of the 8th Scientific Meeting of ISMRM, #861, Denver, 2000.

10. Nishimura DG. Principles of Magnetic Resonance Imaging. Dwight G. Nishimura. Stanford University, 1996.

11. Kim SG, Tsekos NV. Perfusion imaging by a flow-sensitive alternating inversion recovery (FAIR) technique: application to functional brain imaging. Magn Res Med 1997;37:425-435.

12. Zhong J, et al. Quantification of intravascular and extravascular contributions to BOLD effects induced by alteration in oxygenation or intravascular contrast agents. Magn Res Med 1998;40:526-536.

13. Gruetter R, et al. Observation of resolved glucose signal of 1H NMR spectra of the human brain at 4 Tesla. Magn Reson Med 1996;36:1-6.

14. Ogawa S, Lee TM. Magnetic resonance imaging of blood vessels at high fields: in vivo and in vitro measurements and image simulation. Magn Res Med 1990;16:9-18.

15. Ogawa S, Menon RS, Kim SG, Ugurbil K. On the characteristics of functional magnetic resonance imaging of the brain. Annu. Rev. Biophys. Biomol. Struct. 1998;27:447-74.

16. Gati JS, Memon RS, Ugurbil K, Rutt BK. Experimental determination of the BOLD field strength dependence in vessels and tissue. Magn Res Med 1997;38:296-302.

17. Nishimura DG, Irarrazabal P, Meyer CH. A velocity k-space analysis of flow effects in echo-planar and spiral imaging. Magn Reson Med 1995;33:549-556.

18. Meyer CG, Hu BS, Nishimura DG, Macovski A. Fast spiral coronary artery imaging. Magn Reson Med 1992;29:202-213.

19. Yang Y, Glover GH, van Gelderen P, Patel AC, Mattay VS, Frank JA, Duyn JH. A comparison of fast MR scan techniques for cerebral activation studies at 1.5 Tesla. Magn Reson Med 1998;39:61-67.

20. Glover GH, Lee AT. Motion artifacts in fMRI: comparison of 2DFT with PR and spiral scan methods. Magn Reson Med 1995;33:624-635.

21. Marquart M, Birn R, Haughton V. Single- and multiple-event paradigms for identification of motor cortex activation. Am J Neuroradiol 2000;21:94-98.

22. Bandettini PA, Cox RW. Event-related fMRI contrast when using constant interstimulus interval: theory and experiment. Magn Res Med 2000;43:540-548.

23. Righini A, de Divitiis O, Prinster A, Spagnoli D, Appollonio I, Bello L, Scifo P, Tomei G, Villani R, Fazio F, Leonardi M. Functional MRI: primary motor cortex localization in patients with brain tumors. Journal of Computer Assisted Tomography 1996;20(5):702-708.

24. Friston KJ, Williams S, Howard R, Frackowiak RSJ, Turner R. Movement-related effects in fMRI time-series. Magn Res Med 1996;35:346-355.

25. Zeffiro T. Clinical Functional Image Analysis: Artifact detection and reduction. Neuroimage 1996;4:S95-S100.

26. Bandettini PA, Jesmanowicz A, Wong EC, Hyde JS. Processing strategies for time-course data sets in functional MRI of the human brain. Magn Res Med 1993;30:161-173.

27. Hajnal JV, Myers R, Oatridge A, Schwieso JE, Young IR, Bydder GM. Artifacts due to stimulus correlated motion in functional imaging of the brain. Magn Reson Med 1994;31:283-291.

28. Bullmore ET, Brammer MJ, Rabe-Hesketh S, Curtis VA, Morris RG, Williams SCR, Sharma T, McGuire PK. Methods for diagnosis and treatment of stimulus-correlated motion in generic brain activation studies using fMRI. Human Brain Mapping 1999;7:38-48.

29. Ryner LN, Baumgartner R, Somorjai R, Richter W. Widespread respiration-correlated signal changes in BOLD fMRI of resting brain. Proceedings of the 8th Scientific Meeting of ISMRM, #1004, Denver, 2000.

30. Maier SE, Hardy CJ, Jolesz FA. Brain and cerebrospinal fluid motion: real-time quantification with M-mode MR imaging. Radiology 1994;193:477-483.

31. Noll DC, Genovese CR, Vazquez AL, O'Brien JL, Eddy WF. Evaluation of respiratory artifact correction techniques in multishot spiral functional MRI using receiver operator characteristic analyses. Magn Res Med 1998;40:633-639.

32. Biswal B, DeYoe AE, Hyde JS. Reduction of physiological fluctuations in fMRI using digital filters. Magn Res Med 1996;35(1):107-113.

33. Yetkin FZ, Haughton VM, Cox RW, Hyde J, Birn RM, Wong EC, Prost R. Effect of motion outside the field of view on functional MR. Am J Neuroradiol 1996;17:1005-1009.

34. Birn RM, Bandettini PA, Cox RW, Jesmanowicz A, Shaker R. Magnetic field changes in the human brain due to swallowing or speaking. Magn Res Med 1998;40:55-60.

35. Green MV, Seidel J, Stein SD, Tedder TE, Dempner KM, Kertzman C, Zeffiro TA. Head movement in normal subjects during simulated PET brain imaging with and without head restraint. J Nucl Med 1994;35:1538-1546.

36. Ruttimann UE, Andreason PJ, Rio D. Head motion during positron emission tomography: is it significant? Psychiatry Research Neuroimaging 1995;61:43-51.

37. Fitzsimmons JR, Scott JD, Peterson DM, Wolverton BL, Webster CS, Lang PJ. Integrated RF coil with stabilization for fMRI human cortex. Magn Res Med 1997;38:15-18.

38. Debus J, Essig M, Schad LR, Wenz F, Baudendistel K, Knopp MV, Engenhart R, Lorenz WJ. Functional magnetic resonance imaging in a stereotactic setup. Magnetic Resonance Imaging 1996;14(9):1007-1012.

39. Woods RPW, Cherry SR, Mazziotta JC. MRI-PET registration with an automated algorithm. J Comput Assist Tomogr 1993;17:536-546.

40. Biswal BB, Hyde JS. Contour-based registration technique to differentiate between task-activated and head motion-induced signal variations in fMRI. Magn Res Med 1997;38:470-476.

41. Ostuni JL, Santha AK, Mattay VS, Weinberger DR, Levin RL, Frank JA. Analysis of interpolation effects in the reslicing of functional MR images. Journal of Computer Assisted Tomography 1997;21(5):803-810.

42. Kim B, Boes JL, Bland PH, Chenevert TL, Meyer CR. Motion correction in fMRI via registration of individual slices into an anatomical volume. Magn Res Med 1999;41:964-972.

43. Goldstein SR, Baube-Witherspoon ME, Green MV, Eidsath A. A head motion measurement system suitable for emission computed tomography. IEEE Transactions on Medical Imaging 1997;16(1):17-27.

44. Hu X, Le TH, Parrish T, Erhard P. Retrospective estimation and correction of physiological fluctuation in functional MRI. Magn Res Med 1995;24:201-212.

45. Le TH, Hu X. Retrospective estimation and correction of physiological artifacts in fMRI by direct extraction of physiological activity from MR data. Magn Res Medd 1996;35:290-298.

46. Wowk B, McIntyre MC, Saunders JK. K-space detection and correction of physiological artifacts in fMRI. Magn Res Med 1997;38:1029-1034.

47. Buonocore MH, Maddock RJ. Noise suppression digital filter for functional magnetic resonance imaging based on image reference data. Magn Res Med 1997;38:456-469.

48. Cox RW, Jesmanowicz A, Hyde JS. Real-time functional magnetic resonance imaging. Magn Res Med 1995;33:230-236.

49. Voyvodic JT. Real-time fMRI paradigm control, physiology, and behavior combined with near real-time statistical analysis. NeuroImage 1999;10:91-106.

50. Cox RW, Jesmanowicz A. Real-time 3D image registration for functional MRI. Magn Res Med 1999;42(6):1014-1018.

51. Cox RW, Ward BD, Jesmanowicz A. Real-time 3D image registration for fMRI. Proceedings of the 7th Scientific Meeting of ISMRM, Philadelphia, 1999.

52. Chen W, Zhu XH. Suppression of physiological eye movement artifacts in functional MRI using slab presaturation. Magn Res Med 1997;38:546-550.

53. Lee CC, Jack CR, Grimm RC, Rossman PJ, Felmee JP, Ehman RL, Riederer SJ. Real-Time Adaptive motion correction in functional MRI. Magn Res Med 1996;36:436-444.

54. Lee CC, Grimm RC, Manduca A, Felmlee JP, Ehman RL, Riederer SJ, Jack CR. A prospective approach to correct for inter-image head rotation in fMRI. Magn Res Med 1998;39:234-243.

55. Coutts GA, Gilderdale DJ, Chui M, Kasuboski L, DeSouza NM. Integrated and interactive position tracking and imaging of interventional tools and internal devices using small fiducial receiver coils. Magn Res Med 1998;40:908-913.

56. Korin HW, Felmlee JP, Riederer SJ, Ehman RL. Spatial-frequency-tuned markers and adaptive correction for rotational motion. Magn Res Med 1995;33:663-669.

57. Derbyshire JA, Wright GA, Henkelman RM, Hinks S. Dynamic scan-plane tracking using MR position monitoring. J Magn Res Imaging 1998;8:924-932.

58. Sachs TS, Meyer CH, Hu BS, Kohli J, Nishimura DG, Macovski A. Real-time motion detection in spiral MRI using navigators. Magn Res Med 1994;32:639-645.

59. Felmlee JP, Ehman RL, Riederer SJ, Korin HW. Adaptive motion compensation in MRI: accuracy of motion measurement. Magn Reson Med 1991;18:207-213.

60. Ward HA, Riederer SJ, Grimm RC, Ehman RL, Felmlee JP, Jack CR. Prospective multiaxial motion correction for fMRI. Magn Reson Med 2000;43:459-469.

61. Fu ZW, Wang Y, Grimm RC, Rossman PJ, Felmlee JP, Riederer SJ, Ehman RL. Orbital navigator echoes for motion measurements in magnetic resonance imaging. Magn Res Med 1995;34:746-753.

62. Ward HA, Grimm RC, Felmlee JP, Ehman RL, Riederer SJ, Jack Jr CR. Real-time prospective correction of stimulus correlated multiplanar motion during fMRI. Proceedings of the 8th Scientific Meeting of ISMRM, #57, Denver, 2000.

63. Eviatar H, Schattka B, Sharp JC, Rendell J, Alexander ME. Real time head motion correction for functional MRI. Proceedings of the 7th Scientific Meeting of ISMRM, Philadelphia, 1999.

64. Thesen S, Heid O, Mueller E, Schad LR. Prospective acquisition correction for head motion with image-based tracking for real-time fMRI. Proceedings of the 8th Scientific Meeting of ISMRM, #56, Denver, 2000.

65. Thulborn KR. Visual feedback to stabilize head position for fMRI. Magn Res Med 1999;41:1039-1043.

66. Kai J, Shiomi H, Sasama T, Sato Y, Inoue T, Tamura S, Inoue T. Optical high-precision three-dimensional position measurement system suitable for head motion tracking in frameless stereotactic radiosurgery. Computer Aided Surgery 1998;3:257-263.

67. D'Esposito M, Zarahn E, Aguirre GK, Rypma B. The Effect of Normal Aging on the coupling of neural activity to the BOLD hemodynamic response. NeuroImage 1999;10:6-14.

68. The Changing Face of Heart Disease and Stroke in Canada 2000. Ottawa: Heart and Stroke Foundation of Canada, 1999.

69. Johansson BB. Brain plasticity and stroke rehabilitation. Stroke 2000;31:223-230.

70. Weiller C. Imaging recovery from stroke. Exp Brain Res 1998;123:13-17.

71. Rijntjes M, Weiller C, Krams M, Bauermann T, Diener HC, Faiss J. Functional magnetic resonance imaging in recovery from motor stroke. Stroke 1994;25:256.

72. Cramer SC, Nelles G, Benson R, Kaplan JD, Parker RA, Kwong KK, Kennedy DN, Finklestein SP, Rosen BR. A functional MRI study of subjects recovered from hemiparetic stroke. Stroke 1997;28(12):2518-2527.

73. Rosenberg DR, Sweeney JA, Gillen JS, Kim J, Varanelli MJ, O'Hearn KM, Erb PA, Davis D, Thulborn KR. Magnetic resonance imaging of children without sedation: preparation with simulation. J Am Acad Child Adolesc Pyschiatry 1997;36(6):853-859.

74. Gowland C., stratford P, Ward M, Moreland J, Torresin W, Van Hullenaar S, Barreca S, Vanspall B, Plews N. Measuring physical impairment and disability with the Chedoke-McMaster Stroke Assessment. Stroke 1993;24(1):58-63.

75. Staines W.R., McIlroy W.E., Graham S.J., Gladstone D.J., Black, S.E. 2000. Somatosensory extinction of simultaneous bilateral stimuli is associated with decreased activation of somatosensory contralateral cortices: a fMRI study. *Neurology* in press.

76. Field AS, Yens YF, Burdette JH, Elster AD. False activation on BOLD fMRI caused by low-amplitude motion weakly correlated to stimulus. Proceedings of the 8th Scientific Meeting of ISMRM, #1005, Denver, 2000.

77. Psychology Software Tools, Inc., Pittsburgh, PA. See www.pstnet.com for details.

78. Cox RW. AFNI: Software for analysis and visualization of functional magnetic resonance neuroimages. Computers and Biomedical Research 1996;29:162-173.

79. Cox RW, Hyde JS. Software tools for analysis and visualization of fMRI data. NMR in Biomedicine 1997;10:171-178.

80. Wu DH, Lewin JS, Duerk JL. Inadequacy of motion correction algorithms in functional MRI: Role of Susceptibility-Induced Artifacts. JMRI 1997;7:365-370.